applied sciences

MDPI

Article

Integrated Network Reconfiguration and Adaptive Protection Coordination in Active Distribution Systems

Husham Sajir * and Ersagun Kürşat Yaylacı

Department of Electrical & Electronic Engineering, Faculty of Engineering, University of Karabuk, Karabük 78050, Türkiye; ekyaylaci@karabuk.edu.tr
* Correspondence: husham_sl@yahoo.com

Abstract

The widespread use of distributed generation (DG) and renewable energy resources (RES) in contemporary distribution networks significantly alters optimal topology configurations, protection coordination requirements, and network operating conditions. This paper presents a thorough two-stage optimization framework for the concurrent optimization of adaptive protection coordination and distribution network reconfiguration (DNR) in renewable-integrated active distribution systems. The framework addresses the dual issues of ensuring reliable relay coordination under dynamically fluctuating fault current levels caused by variable DG output and minimizing active power losses through optimal switch reconfiguration. The Harmony Search Algorithm (HSA) is used in Stage I minimize active power losses at four loading levels (100–220% of nominal demand), subject to radiality, voltage and branch-current constraints, thereby determining the ideal radial network topology. To satisfy all Coordination Time Interval (CTI) constraints, Stage II uses a hybrid Genetic Algorithm–Sequential Quadratic Programming (GA–SQP) approach that combines the precise local refinement of SQP with the global exploration of GA to determine the optimal Time Dial Settings (TDS) of directional overcurrent relays for the reconfigured network. For any resulting radial topology, an automated graph analysis algorithm dynamically finds primary–backup relay pairs, eliminating the need for human operator intervention in the protection coordination loop. Relay settings are determined for each loading level using the DG fault-current contributions obtained from a positive-sequence short-circuit analysis of a balanced three-phase fault at the midpoint of each line. Network reconfiguration lowers the active power loss by 21.42%, 28.24%, 31.70%, and 33.88%, respectively, while maintaining the minimum voltage above 0.90 pu, according to simulations of the DG-integrated IEEE 33-bus system at four loading levels (100–220% of nominal demand); the same configurations are obtained in repeated HSA runs with different random seeds. The DG units must be included in the reconfiguration problem, since an optimal configuration without them increases the loss by 33.9% when they are added. Relay coordination is linear in the TDS variables for fixed pickup currents; it is solved by the hybrid GA–SQP and validated against the exact linear-programming optimum: the total primary operating time of the 32 relays is 18.14–19.47 s (0.57–0.61 s per relay; maximum 1.36 s), and all 31 primary–backup pairings satisfy a CTI of 0.2 s. This per-relay time is less than the figures published for standalone GA (3.71 s) and HHO-SQP (1.33 s) coordination at nominal loads. The primary contribution of this work is the integration of protection coordination and reconfiguration into a single framework.

Keywords: distribution network reconfiguration; adaptive protection coordination; renewable energy integration; genetic algorithm and sequential quadratic programming optimization; smart grid operation

Check for updates

Academic Editor: Roberto Zivieri

Received: 15 October 2026
Revised: 4 November 2026
Accepted: 5 November 2026
Published: 18 November 2026

Copyright: © 2026 by the authors. Licensee MDPI, Basel, Switzerland. This article is an open access article distributed under the terms and conditions of the Creative Commons Attribution (CC BY) license.

1. Introduction

Renewable energy has emerged as a modern solution to end the severe environmental damage caused by carbon-based energy sources, which have spread at an unprecedented pace [1]. Distribution networks (DN) at all voltage levels are being transformed from passive, unidirectional delivery systems into active, bidirectional energy infrastructure by the integration of photovoltaic (PV) systems, wind turbines, and other DG technologies [2]. The evolution of networks into smart networks is a necessary component of this transformation. Still, it presents significant technical challenges across various aspects of the distribution system, including operation, planning, and protection. Modern active distribution networks (ADNs) require increased efficiency to keep pace with technological advancements. Therefore, the network topology must be optimized to adequately support this increased efficiency. Traditionally, DNR and protection coordination have been treated as distinct, independent issues. Voltage profiles are optimized, and power is reduced by implementing DNRs via switching-mode adjustments, while protection devices are coordinated independently based on the fixed network topology [3]. Discrete ADNs are an inadequate methodology in any form for highly integrated renewable energy sources, since the error current and optimal structure are constantly fluctuating with daily demand and changing weather conditions, leading to changes in DG outputs [4]. Radial topology arises by determining the closed and open states of the links and dividing the switches via DNR, while minimizing a target that adheres to operational constraints, such as power loss. Metaheuristic optimization algorithms are fundamental to network development. HSA is an exceptional and effective means of DNR through the musical improvisation process, demonstrating its reliability through direct application, a tight balance between local exploitation and global exploration, and the minimum control criteria [5].

In Active DN, protection coordination requires configuring overcurrent relays to ensure that primary relays isolate faults as quickly as possible. On the other hand, in the case of a primary relay failure, backup relays function within a secure time margin (CTI). The addition of DG units further complicates this need. The primary–backup relay relationships are affected by different network topologies resulting from reconfiguration, and changes in DG output alter fault current levels at relay locations [6]. The network operates in accordance with predefined operational standards. At the same time, the protection system coordinates protective devices and distributed generation to maintain a secure and reliable operating state under both normal and abnormal conditions. The dependable operation of ADNs depends on scalable protection coordination, which dynamically adjusts relay settings based on the current network status [7,8].

Relay setup optimization is a nonlinear, non-convex programming problem with several coordination constraints. Although they can exhaustively explore the solution space, standalone metaheuristic techniques such as GA may not converge to precise, workable solutions. SQP and other gradient-based techniques provide precise local convergence. However, when the situation is not convex, they frequently converge to unsatisfactory local optima and are sensitive to initial conditions. The best features of both approaches are combined in the hybrid GA-SQP technique. SQP is then used to refine this solution toward local optimality while precisely meeting all operational constraints once the GA has produced a high-quality, viable starting solution [9].

The integration of cutting-edge sensing, communication, computation, and control technologies enables smart grids to operate autonomously. Consequently, automated decision-making and real-time monitoring can be achieved without human intervention [3,10]. The efficiency, dependability, and resilience of the system are directly affected by the smart grid's ability to optimize network topology and protection coordination simultaneously.

Smart grids require an automated framework capable of integrated optimization without human involvement to function autonomously.

DNR, adaptive protection coordination, integration of RES, and smart grid operation are among the closely related issues examined in this paper. The paper uses a two-stage optimization methodology to address these interrelated problems; each stage is intended to handle particular parts of the overall problem in a coordinated manner. The suggested method is implemented and evaluated on a typical IEEE 33-bus active distribution system with dispersed generation, thereby enabling assessment of its efficacy in a practical setting. The framework incorporates the HSA for topology optimization, alongside a hybrid GA–SQP method for relay coordination, and is linked by an automated graph-analysis algorithm that dynamically identifies primary–backup relay pairs for any network configuration. Load demand is represented by four loading levels (100–220% of nominal demand), and the fault-current contribution of each DG type is obtained from its short-circuit model. The proposed GA-SQP hybrid method yields a total primary relay operating time of 18.40 s for 32 coordinated relays (0.575 s per relay) at nominal loading, which coincides with the exact linear-programming optimum; comparison with previously published results is provided for reference only. This result shows that the approach attains the exact optimum for the 33-bus system studied; its scalability to larger networks remains to be investigated.

The main contributions of this paper are:

- HSA for optimal distribution network reconfiguration utilizing a hybrid GA–SQP methodology to ascertain the optimal time-delay settings of directional overcurrent relays.
- Attaining synchronized functionality between network topology and protection settings, wherein the relay parameters derived from GA–SQP optimization fulfills the protection coordination requirements linked to the network configuration established by the HSA-based reconfiguration process.
- Relative to [1,11–13], the novelty of this work lies in the closed link between network topology and protection settings: relay settings are recomputed for every reconfigured topology and loading level through an automatic primary–backup pair identification algorithm, and the trade-off between power loss and relay operating time across topologies is quantified.
- Delivering a thorough evaluation framework via extensive simulations on the IEEE 33-bus distribution system with distributed generation to illustrate the efficacy of the proposed method in enhancing system performance while ensuring secure relay coordination.

The subsequent sections of this paper are structured as follows: Section 2, literature review and theoretical background. Section 3 presents the problem formulation. Section 4 describes the proposed two-stage optimization framework. Section 5 presents and discusses the simulation results. Finally, Section 6 concludes the paper.

2. Literature Review and Theoretical Background

2.1. Distribution Network Reconfiguration

DNR refers to the procedure of modifying the open/closed status of switches within a distribution network to alter its topology while maintaining the radial (tree) configuration essential for standard protection functionality. A standard distribution network comprises two types of switches: sectionalizing switches, typically closed, located on main feeders and lateral branches; and tie switches, generally open, that link various feeders or sections. To modify the network topology to achieve various operational objectives, one may open certain sectionalizing switches and close specific tie switches. Ensure that no loops form and that all loads remain connected [14,15].

The main goals of DNR are to reduce active power loss [3], reactive power loss [16], bus voltage profile improvement, and voltage deviation reduction, to balance the load among feeders [11,17], to improve reliability, to restore service after faults, and to lower greenhouse gas emissions [18]. In the context of ADNs with DG, DNR can also be used to make the most of DG, reduce the need to curtail renewable energy, and improve the charging and discharging cycles of energy storage systems [11,19].

2.1.1. Mathematical Formulation

Mathematically, the DNR problem is formulated as a Mixed-Integer Nonlinear Programming (MINLP) problem. The general loss minimization formulation is:

$$minP_{loss} = \sum (i,j) \in L\, r_{ij} \times I_{ij}^2 \quad (1)$$

Subject to:

- Radial (spanning tree) topology: the graph G (N, L_{closed}) must be a tree with |N| − 1 closed branches.
- Power flow equations: active and reactive power balance at every bus.
- Voltage limits: $V_{min} \leq V_i \leq V_{max}$ for all buses *i*.
- Current limits: $I_{i,j} \leq I_{max,\, i,j}$ for all branches (*i*,*j*).
- Switch state: α_{ij} {0, 1} for all switchable branches.

The nonlinearity arises from the power-flow equations and the current-voltage relationship. The discrete nature of switch states leads to an exponentially growing combinatorial solution space as the number of switches increases. A network of N_s switches can have 2^{N_s} possible groups of switches, but only a subset of those is radial and viable. In standard DN with five or more tie switches, the search space ranges from 32 to over a million configurations [2].

2.1.2. Solution Methods

In early DNR techniques, heuristic branch-exchange methods that iteratively exchange switch states based on local improvement criteria were utilized [4]. These methods are computationally efficient but highly dependent on local optima and cannot guarantee global optimality. Constructive heuristics start from an empty configuration and generate the optimal one by applying rules, for example, minimal loss increment per switching operation [20].

Mathematical programming methods like Mixed-Integer Linear Programming (MILP) and convex relaxations can provide optimality guarantees, but they suffer from scalability issues for large networks [21]. The MILP formulation employs the linearized DistFlow model to compute power flow, yielding a manageable mixed-integer linear program at the expense of reduced accuracy. Second-Order Cone Programming (SOCP) relaxations are closer approximations in terms of convexity [22].

Metaheuristic algorithms are popular for DNR because they can explore large combinatorial spaces without gradient information. To move populations toward better solutions, GA uses crossover and mutation operators to represent switch states as binary chromosomes [11]. With velocity updates based on both individual and collective optimal positions, Particle Swarm Optimization (PSO) models change states as particles move in continuous space [1]. Pheromone trails are employed in Ant Colony Optimization (ACO) to direct the search toward favorable regions and gradually construct solutions [23]. The Lévy flight pattern is used by Cuckoo Search (CS) to efficiently and swiftly search huge solution spaces [2]. The Firefly Algorithm (FA) guides a population's evolution using attraction mechanisms based on light intensity (fitness) [24].

2.1.3. Harmony Search Algorithm for DNR

The art of musical improvisation inspires the HSA. Similar to how musicians tune the pitches of their instruments to create a pleasing harmony, HSA tunes solution variable values to minimize an objective function. The algorithm has several properties that make it especially suitable for the DNR problem:

- Simple parameter structure: HSA is characterized by its simplicity in terms of parameters, as it only requires three main control parameters: Harmony Memory Consideration Rate (HMCR), Harmony Memory stores (HMS), and Pitch Adjustment Rate (PAR). This makes it easier to tune and apply than other optimization algorithms that require 5 or more parameters, such as GA or PSO.
- HSA is particularly well-suited to discontinuous or noisy objective functions because it does not require gradient information.
- Natural handling of discrete variables through the pitch adjustment mechanism.
- Memory-based search: the best HMS solutions found so far, providing a form of population diversity maintenance.
- Convergence speed: the combination of memory consideration (exploitation) and random selection (exploration) typically achieves rapid convergence.

2.2. Adaptive Protection Coordination in Active Distribution Networks

Conventional DNs are protected by overcurrent relays, fuses, and reclosers, arranged in a hierarchical coordination scheme. The principle of basic coordination states that the device closest to the fault should operate first to insulate the smallest faulted area. If the primary fails, the next upstream device (the backup) should take over with a time delay. The CTI enforces this hierarchy by showing the minimum time required between the primary and backup relays.

The operating time for directional overcurrent relays that follow the IEC 60255 standard [25] for inverse-time characteristics is

$$t_i = A \times \frac{TDS}{\left[\left(I_f / CPS_i\right)^B - 1\right]} \tag{2}$$

(IEC Standard Inverse: A = 0.14, B = 0.02)

where TDS is the Time Multiplier Setting, CPS is the Current Pickup Setting, I is the fault current seen by the relay, and A and B are curve shape constants. The coordination constraint for a primary relay p and backup relay b is:

$$t_{b,f} - t_{p,f} \geq CTI \text{ for all fault location } f \tag{3}$$

Typical CTI values range from 0.2 s to 0.5 s, accounting for relay measurement errors (±5%), circuit breaker operating time (~80 ms), and safety margins [6,12]. In this work, the CTI of 0.2 s, which is commonly adopted for digital relays, is used in all reported results; a CTI of 0.3 s is also examined as a sensitivity case.

2.2.1. Protection Challenges in Active Distribution Networks

The integration of DG into DN creates several well-documented challenges for conventional protection schemes [12].

2.2.2. Protection Blinding

When a DG unit sends current to a fault on an upstream feeder, the upstream relay sees less fault current than it would without the DG. This can reduce the amount of visible fault current, causing the relay to operate more slowly or, in the worst cases, fail to operate

(blinding). The blinding effect is strongest when the DG accounts for a large share of the total fault current and when the relay CPS is set close to the load current.

2.2.3. False Tripping and Nuisance Tripping

When problems occur on nearby feeders, distributed generation units may cause overcurrent relays on operational feeders to trip incorrectly. If a fault on feeder A causes a distributed generator on feeder B to send current through the relay on feeder B (toward the fault on feeder A), the relay on feeder B may trip even though feeder B is still working, as shown in Figure 1. This phenomenon, known as sympathetic or nuisance tripping, presents considerable difficulties in meshed networks or those featuring multiple distributed generation interconnection points.

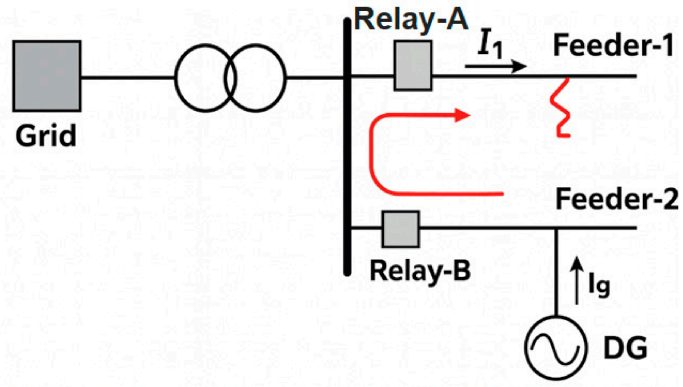


Figure 1. Impact of DG deployment on a traditional distribution grid [25].

2.2.4. Loss of Coordination Selectivity

DG can alter the magnitude and direction of fault currents, making it difficult for primary and backup relays to coordinate. In some cases of faults and combinations of distributed generation output, a backup relay intended to operate only when the primary relay fails may operate faster than the primary relay [26,27]. Because of the lower selectivity, a larger portion of the network trips than necessary are required, causing outages over a larger area [8].

2.3. Renewable Energy Integration and Its Impact on Distribution Networks

DG units incorporated into supply chains can be classified based on their primary energy source and interfacing technology. Synchronous generators, supplied by small gas turbines, diesel engines, or micro-hydro turbines, are directly connected to the network and exhibit behavior similar to standard-sized generators during faults, delivering 5–10 times their rated current [5]. The doubly fed induction generators (DFIGs) used in different wind turbine concepts can carry (3–5) times the rated current during faults until the protection systems restore the current to the rated value [20].

Inverter-interfaced distributed generators (IIDGs), such as PV systems and full-converter wind turbines, exhibit fundamentally distinct fault characteristics. The power electronic inverter restricts the output current to 1.1–3.0 times the rated current to safeguard the semiconductors from thermal degradation. The minimal fault-current contribution, although safeguarding the inverter, results in IIDGs being able to sufficiently activate the protection relay during a fault, which may lead to protection blinding [28].

Impact of Distributed Generation on Fault Current: The integration of DG units alters the fault current distribution throughout the network in topology-dependent ways. For a three-phase bolted fault at location f in a network with DG units at buses d_1, d_2, ..., d_3:

$$I_{f,relay} = I_{f,grid} + \sum_{k=1}^{n} \delta_k \times I_{f,DGk} \quad (4)$$

where $I_{f,grid}$ is the grid contribution to the fault current at the relay location, δ_k is a dimensionless DG contribution factor $0 \leq \delta_k \leq \delta_{max}$, and $I_{f,DGk}$ is the fault current contribution from the k-th DG unit. The contribution factor δ_k depends on the electrical distance between the DG and the fault location, the network topology (which changes with reconfiguration), and the DG operating state.

For synchronous DGs and DFIGs, $\delta_{max} \approx 5$–10 during the sub-transient period (first few cycles). For IIDGs, $\delta_{max} \approx 1.1$–3.0 depending on the inverter control strategy. The uncertainty in δ arises from the variability of DG output; a PV system operating at 10% capacity during cloudy conditions contributes far less fault current than the same system at full output [29,30].

2.4. Optimization Methods for Relay Coordination

The Protection Coordination Problem (PCP) is the optimization problem of finding relay settings (TDS and CPS) that minimize total relay operation time, subject to CTI constraints, across all primary–backup pairs and all fault locations. It is formally stated as:

$$min\ T = \sum_{i=1}^{N} t_{p,i} \quad (5)$$

Subject to:

$$t_{b,j,f} - t_{p,i,f} \geq CTI \quad \forall (i,j) \in pairs, f \in faults \quad (6)$$

$$TDS_{min} \leq TDS_i \leq TDS_{max} \quad (7)$$

$$OLF \times I_{N,i} < CPS_i < I_{min,f,i}/3 \quad (8)$$

The PCP is nonlinear due to the inverse-time relay characteristic and non-convex due to the interaction between TDS and fault current in the operating time expression. For a network with N relays and fault locations, the PCP has N continuous TDS variables, N discrete CPS variables, and N × F coordination constraints. The OLF is standard for Overall Load Factor (assuming the load current could be 25% higher than its rated normal value $I_{N,i}$ before the relay is allowed to trip). For typical distribution networks, N ranges from 5 to 50 and F from 10 to 200 [1].

2.4.1. Metaheuristic Approaches

Metaheuristic methods have been widely used for the PCP because they can explore the non-convex solution space globally [31]. GA encodes relay configurations as chromosomes and evolves populations through selection, crossover, and mutation operators. PSO represents relay configurations as particle positions and advances the swarm towards optimal solutions [11]. Recent applications encompass NLP [32], Teaching–Learning-Based Optimization [33], Biogeography-Based Optimization [24], and the Salp Swarm Algorithm (SSA) [34].

A consistent observation across these studies is that metaheuristics outperform LP for joint TDS/CPS optimization and circumvent the local optima issue inherent in NLP [35]. Nevertheless, metaheuristics may fail to satisfy the exact constraints mandated by the PCP; CTI constraints may be infringed by small amounts (typically 10–50 ms), which are deemed unacceptable in practice.

2.4.2. The GA–SQP Hybrid

This paper presents a hybrid GA–SQP approach that integrates the global exploration capabilities of GA with the meticulous local optimization of SQP. The principal observation is that SQP convergence to the global optimum is assured when initiated sufficiently near it; however, the basin of attraction for the global optimum may be limited in the case of the non-convex PCP. GA effectively locates a point within or adjacent to this basin, from which SQP converges accurately.

SQP addresses a general NLP by iteratively resolving Quadratic Programming (QP) subproblems derived from quadratic approximations of the Lagrangian and linearization of the constraints [32]. At each iteration k, the quadratic programming subproblem is:

$$min\frac{1}{2}d^{T}H_{k}d + \nabla f(x_{k})^{T}d \quad (9)$$

Subject to:

$$\nabla c_{i}(x_{k})^{T}d + c_{i}(x_{k}) = 0 \text{ (equality constraints)} \quad (10)$$

$$\nabla c_{j}(x_{k})^{T}d + c_{j}(x_{k}) \geq 0 \text{ (Inequality constraints)} \quad (11)$$

where H_k is a positive definite approximation of the Lagrangian Hessian, updated using the Broyden-Fletcher-Goldfarb-Shanno (BFGS) formula. The search direction d_k is the QP solution. A line search along d_k ensures a sufficient decrease in the merit function $\phi(x) = f(x) + \sum_i \mu_i |c_i(x)|$, where μ_i are updated penalty parameters to ensure constraint feasibility. Convergence is achieved when the Karush-Kuhn-Tucker (KKT) optimality conditions are satisfied with the specified tolerance.

The advantage of SQP over other NLP methods for the PCP is its ability to handle inequality constraints directly without penalty functions (which introduce numerical difficulties), its super-linear convergence rate near the optimum, and its availability in high-quality software implementations.

2.5. Smart Grid

A smart grid is an electricity supply network that employs digital communication technology to identify and respond to local fluctuations in consumption, facilitating bidirectional communication between the utility and its customers and automating distribution management functions [3]. The distinguishing characteristics of smart grids compared to conventional grids include advanced metering infrastructure (AMI), distribution automation (DA), demand response (DR), integration of distributed energy resources (DER), real-time monitoring and control, and self-healing capabilities [1,2].

From the standpoint of distribution network management, smart grid operation entails the ability to reconfigure the network in near-real time in response to prevailing operating conditions, automatically adjust protection settings in response to changes in network topology, and optimize the balance between network efficiency and protection reliability without manual operator involvement. The proposed two-stage framework precisely offers these capabilities [1].

3. Problem Formulation

The distribution network is represented as a directed graph G = (N, L), where N denotes the set of buses, and L signifies the set of branches, as shown in Figure 2. The network comprises a substation bus (root node), load buses, DG buses, and switchable branches. The binary vector $\alpha = [\alpha_1, \alpha_2, \ldots, \alpha_{|L|}]$ represents the operational status of each branch: $\alpha_{ij} = 1$ indicates that the branch (i,j) is closed, while 0 signifies that it is open [26].

The DistFlow branch flow model delineates the power flow equations for each loading level s:

$$P_{ij,s} = \sum_{k:(j,k)\in L} P_{jk,s} + P_{L,j,s} - P_{DG,j,s} + r_{ij} I_{ij,s}^2 \tag{12}$$

$$Q_{ij,s} = \sum_{k:(j,k)\in L} Q_{jk,s} + Q_{L,j,s} - Q_{DG,j,s} + x_{ij} I_{ij,s}^2 \tag{13}$$

$$V_{j,s}^2 = V_{i,s}^2 - 2\left(r_{ij} P_{ij,s} + x_{ij} Q_{ij,s}\right) + \left(r_{ij}^2 + x_{ij}^2\right) I_{ij,s}^2 \tag{14}$$

$$I_{ij,s}^2 = \left(P_{ij,s}^2 + Q_{ij,s}^2\right) / V_{i,s}^2 \tag{15}$$

where P_{ij}, Q_{ij} are active and reactive power flows on the branch (i,j); P_L, Q_L and P_{DG}, Q_{DG} are load and DG active and reactive powers; V_i is the bus voltage magnitude; r_{ij}, x_{ij} are branch resistance and reactance; and s indexes the loading level.

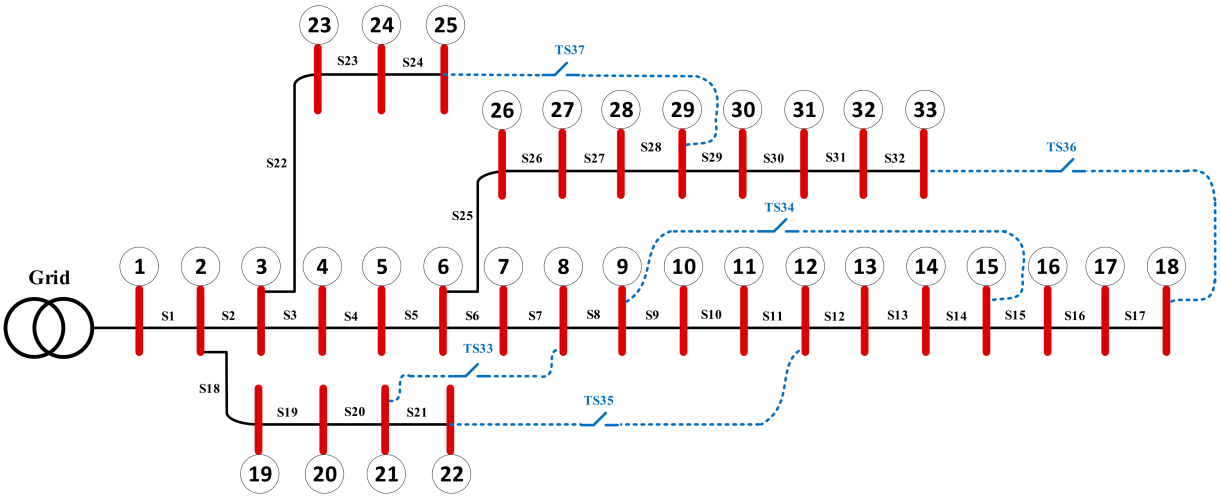


Figure 2. Modeled test system of 33 buses.

3.1. Stage I: DNR Objective and Constraints

The Stage I objective function is designed to minimize the total active power loss across Ns operating scenarios, where each scenario corresponds to a network loading level (100%, 140%, 180%, or 220% of the nominal demand).

$$minf_1 = \sum_{s\in S} \pi_s \times \sum_{(i,j)\in L} \alpha_{ij} \times r_{ij} \times I_{ij,s}^2 \tag{16}$$

where π_s is the weight of loading level s; each level is optimized in a separate run, so that Ns = 1 and, with uniform weights, $\pi_s = 1/N_s$. The load at each bus is scaled by the corresponding loading factor, and the DG units operate at their rated set points; no probabilistic sampling of the load is applied. The constraints are as follows:

- Radiality: the graph G (N, {(i,j): $\alpha_{ij} = 1$}) must be a spanning tree.
- Voltage limits: $V_{min} \le V_{i,s} \le V_{max}$ for all i ∈ N, s ∈ S. ($V_{min} = 0.90$, $V_{max} = 1.05$ pu).
- Current limits: $I_{ij,s} \le I_{max,ij}$ for all (i,j) ∈ L, s ∈ S.
- DG injection: $\sum P_{DG,i} < \sum P_{L,n,s} + P_{loss,s}$ to prevent reverse power flow to the grid.

Scenario treatment. The scenario set in Equation (16) comprises the four loading levels considered in this study (Ns = 4), covering the demand range from 100% to 220% as indicated by the Latin Hypercube Sampling coverage. No additional random samples are drawn within each loading level. At each level, the load at each bus is scaled by the corresponding loading factor, and the DG units are modeled at their rated active-power set points. The variation in the DG contribution is therefore represented through the fault-current model of each DG type in Stage II, and not through sampled output profiles. Since

the four loading levels are optimized independently, each HSA run involves a single scenario ($\pi s = 1$). Equation (16) applies when several scenarios are combined into a single run. The uniform weighting $\pi s = 1/Ns$ of Equation (16) applies when several scenarios are combined in one run.

3.2. Stage II: Relay Coordination Objective and Constraints

Given the optimal topology α^* from Stage I and the resulting fault currents $I_{f,i}$ (computed by short-circuit analysis for α^*, at each loading level, with the DG contributions obtained from the short-circuit models of the DG units), Stage II minimizes total primary relay operating time:

$$minf_2 = \sum_{s \in Sf} \pi'_s \times \sum_{i=1}^{N} t_{p,i,s} \tag{17}$$

where s denotes the loading level, for which the fault currents are evaluated separately, π'_s is the weight of that loading level (equal to 1), and $t_{p,i,s}$ is the operating time of the primary relay *i* at loading level s, computed from the IEC characteristic as showing in Table 1:

$$t_{p,i,s} = \frac{A \times TDS_i}{\left[\left(I_{f,i,s}/CPS_i\right)^B - 1\right]} \tag{18}$$

Table 1. OCR classification [25].

Type of OCR	Equation of Operation Time
Normally inverse	$T_i^m = \frac{0.14}{\left(\frac{I^i_{max.Load}}{I^i_p}\right)^{0.02} - 1} TDS_i^m$
Very inverse	$T_i^m = \frac{13.5}{\left(\frac{I^i_{max.Load}}{I^i_p}\right) - 1} TDS_i^m$
Extremely inverse	$T_i^m = \frac{80}{\left(\frac{I^i_{max.Load}}{I^i_p}\right)^2 - 1} TDS_i^m$
Ultra-extremely inverse	$T_i^m = \frac{120}{\left(\frac{I^i_{max.Load}}{I^i_p}\right) - 1} TDS_i^m$

Subject to the following constraints:

- CTI constraint: $t_{b,j,f,s} - t_{p,i,f,s} \geq$ CTI for all (i,j) $\in$ pairs, f $\in$ faults, s $\in$ Sf. CTI = 0.2 s (0.3 s as sensitivity case).
- TDS bounds: $TDS_{min} \leq TDS_i \leq TDS_{max}$. ($0.05 \leq TDS_i \leq 1.0$).
- CPS sensitivity: $CPS_i < I_{min,f,i}/3$ (Relay must detect minimum fault current).
- CPS overload: $CPS_i >$ OLF $\times I_{L,max,i}$ (relay must not trip under maximum load, OLF = 1.25).
- Operating time: $t_{min} \leq t_i \leq t_{max}$. ($t_{min} = 0.05$ s).
- Decision variables and solution method. Although CPS_i is bounded by the sensitivity and overload constraints above, in the reported simulations the pickup currents are fixed at $CPS_i = 1.25\ I_{L,max,i}$ (rounded to the nearest 5 A, with a minimum of 10 A), which satisfies both constraints; the TDS_i are therefore the only decision variables. For fixed pickup currents, $t_{p,i}$ is proportional to TDS_i, so the objective and the CTI constraints are linear, and the problem could be solved directly by linear programming, which is used here as the exact benchmark (Section 5). The hybrid GA–SQP is retained as a general solver that remains applicable when CPS_i is also optimized, in which case the problem becomes nonlinear and non-convex, and its solutions are validated against the LP optimum.

4. Proposed Two-Stage Optimization Framework

The proposed framework divides the joint DNR–protection coordination issue into two sequential phases linked by the automated relay identification algorithm. The problem's conditional framework warrants decomposition: the relay coordination constraints depend on the network topology via fault currents and relay pairs; once the topology is established, the relay coordination issue is unaffected by the reconfiguration variables. This conditional independence allows the two stages to be addressed sequentially. The sequential solution, however, is not guaranteed to be jointly optimal, because the loss-optimal topology does not necessarily minimize the relay operating time; a near-optimal topology reduces the total primary operating time by 8.9% at the expense of a 2.2% increase in losses.

The comprehensive framework flowchart unfolds as follows: Stage I (HSA) determines the optimal topology α^* the automated algorithm establishes primary–backup pairs for α^* short-circuit analysis calculates fault currents for α^* considering DG uncertainty, Stage II (GA–SQP) derives optimal TDS* and CPS*; the integrated solution (α^*, TDS*, CPS*) is validated and documented.

4.1. Stage I: Harmony Search Algorithm

4.1.1. HSA Mechanics

The HSA preserves a Harmony Memory (HM) consisting of HMS = 30 candidate switch configurations, with each harmony denoting a vector of 5 open switches chosen from the 37 branches of the IEEE 33-bus distribution network, as illustrated in Figure 3.

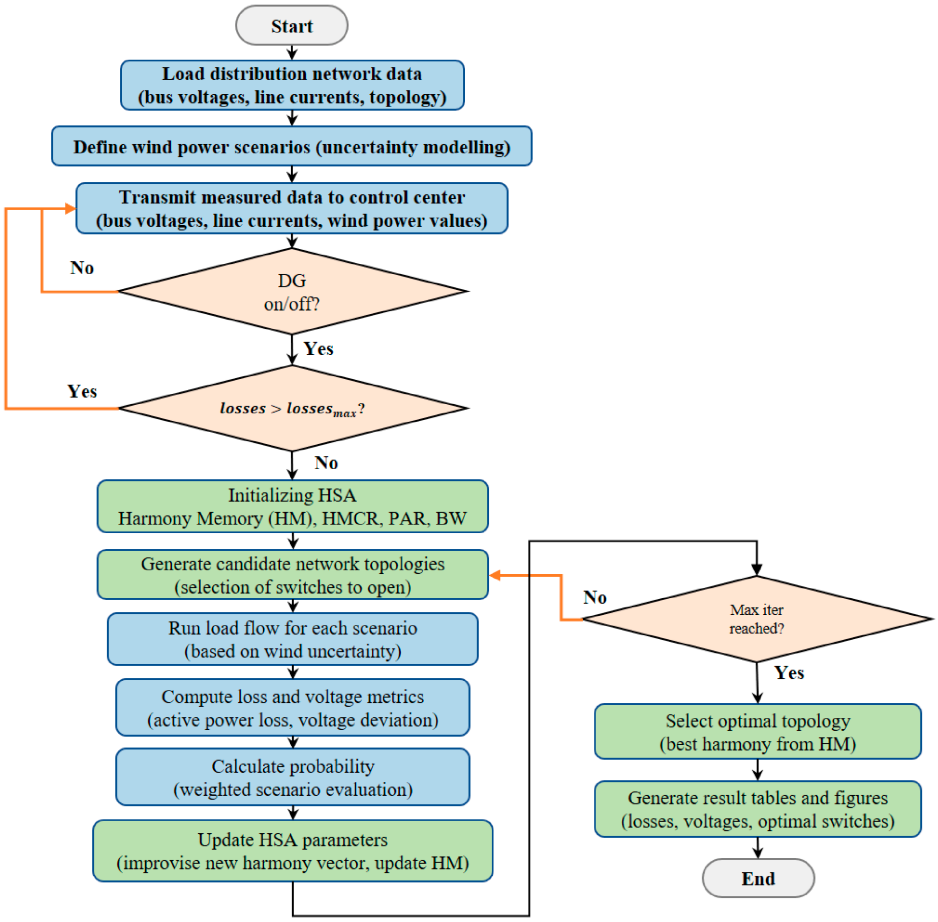


Figure 3. Mechanics of HSA.

The algorithm initializes HM by randomly generating HMS radial configurations through uniform integer sampling within the branch index range (1, 37, i.e., 32 sectionalizing and 5 tie branches), confirming radiality via the island detection criterion:

$$Radial \iff N_{islands} = 1 \; and \sum_{i=1}^{N_{br}} s_1 = N_{bus} - 1 \tag{19}$$

where $s_i \in \{0, 1\}$ is the status of the branch *i*. For each valid configuration, the load flow is solved using the Newton–Raphson method via MATPOWER across all N_s wind scenarios, with DG output scaled according to each scenario's capacity factor. The fitness of each harmony is computed as the probability-weighted sum:

$$F(x) = \sum_{s=1}^{N_s} \pi_s \left(\frac{P_{loss,s}(x)}{P_{loss,s}^{ref}} + \frac{VD_s(x)}{VD_s^{ref}} \right) + M.1\,[non - radial] \tag{20}$$

where $P_{loss,s}(x) = \sum_{i=1}^{N_{br}} Re(S_{loss,i})$ is the total active power loss under the configuration *x* and scenario (s), $VD_s(x) = \sum_{j=1}^{33} |1 - V_j|$ is the total voltage deviation; the superscript ref denotes the base configuration without reconfiguration, π_s is the probability weight of the scenario (s) satisfying $\sum_{s=1}^{N_s} \pi_s - 1$, and $M - 10^3$ is the penalty coefficient assigned to any non-radial or islanded configuration.

4.1.2. Improvisation Mechanism for Binary Variables and Their Parameters

With each repetition, a fresh harmony is created. For every decision variable $j \in (1–5)$ (the index of an activated switch), a value is selected from a randomly chosen harmony within the harmony memory (HM) with a probability of $HMCR = 0.95$; if not, a branch index is uniformly sampled from (1, ..., 37). If the memory-consideration phase is activated, a pitch modification is implemented with a likelihood of PAR.

$$x_j^{new} = \min(37, \max(1, x_i + \delta)),\ \delta \in \{-1,\ 0, +1\} \tag{21}$$

where δ is drawn uniformly, and PAR decreases linearly from 0.10 to 0.05 over the iterations:

$$PAR(t) = PAR_0 + \left(PAR_f - PAR_0\right) \cdot \frac{t}{N_{\max}} \tag{22}$$

with PAR_0 set at 0.10 PAR_f at 0.05, and $NI = 3000$. Duplicate switch indices within a harmony are eliminated and substituted with fresh random indices, ensuring that each harmony has five unique open switches. The novel harmony is assessed using a power flow and supersedes the least favorable harmony in the memory (HMS = 30) if it offers a lower cost and is not currently stored; hence, the quality of the memory consistently improves over the iterations. The search concludes after 3000 iterations or after 600 iterations without enhancement, and the optimal harmony is polished with a final single-switch exchange, as illustrated in Table 2 and Figure 3.

Table 2. HSA control parameters for Stage I.

Parameter	Symbol	Value	Rationale
Harmony Memory Size	HMS	30	Balance exploration and memory quality
Consideration Rate	HMCR	0.95	High exploitation of good solutions
Pitch Adjustment Rate	PAR	0.10 → 0.05	Linear decrease
Improvisation Cycles	NI	3000	Convergence for 33-bus networks with early stopping
Load levels	Ns	4	Deterministic loading levels (100–220% of nominal demand)
Penalty Coefficient	M	10^3	Strong constraint enforcement

4.2. Stage II: Hybrid GA–SQP

4.2.1. GA Phase: Global Search

The GA maintains a population of P = 100 relay setting vectors, each encoding [TDS_1, ..., TDS_N, CPS_1, ..., CPS_N]. *TDS* variables are real valued in [TDS_{min}, TDS_{max}]. *CPS* values are selected from discrete sets based on load current: $CPS_i \in$ {CPS values satisfying $OLF \times I_{L,max,i} < CPS_i < I_{min,f,i}/3$}.

The GA fitness function penalizes CTI violations:

$$F_{GA}(TDS, CPS) = \sum_s \pi'_s \sum_i t_{p,i,s} + M_1 \sum_{(i,j),f,s} max\left(0, CTI - \left(t_{b,j,f,s} - t_{p,i,f,s}\right)\right) \quad (23)$$

with $M_1 = 10^3$ as the CTI violation penalty. The evolutionary operators are as follows:

- Selection: Tournament selection (tournament size = 3) with elitism (top 5% preserved).
- Crossover: Simulated Binary Crossover (SBX) with $P_c = 0.85$, distribution index $\eta_c = 20$ SBX for real-valued variables mimics single-point crossover while respecting variable bounds and preserving diversity near good solutions.
- Mutation: Polynomial mutation with $P_m = 1/n$, distribution index $\eta_m = 20$. The distribution index controls spreading mutation. Larger values concentrate mutations near the current value (exploitation); smaller values spread them more widely (exploration).
- Termination: Max 500 generations or stagnation ($<10^{-6}$) improvement over 30 generations).
- Multi-start: 5 independent GA runs with different random seeds; best solution $x_{0,GA}$ selected across all runs to reduce dependence on initial conditions.

4.2.2. SQP Phase: Local Refinement

The best GA solution $x_{0,GA}$ is provided as the starting point for MATLAB's 2023b fmincon with the 'sqp' algorithm option. The SQP phase solves the full NLP precisely:

- Objective: minimize $\sum_s \pi'_s \sum_i t_{p,i,s}$ (expected primary relay operating time).
- Inequality constraints: $t_{b,j,f,s} - t_{p,i,f,s} \geq$ CTI for all pairs, faults, and scenarios.
- Bound constraints: $TDS_{min} \leq TDS_i \leq TDS_{max}$, $CPS_{min,i} \leq CPS_i \leq CPS_{max,i}$.
- Convergence tolerances: constraint tolerance and step tolerance of 10^{-8}, as showing in Table 3.

The SQP stage employs sequential quadratic programming with a quasi-Newton Hessian approximation and the IEC Standard Inverse relay characteristic. It is initialized from the best GA solution, with the constraint and step tolerances listed in Table 3. Because the problem is linear in the TDS variables, all multi-start SQP runs converge to the same objective value, which coincides with the exact linear programming optimum.

Table 3 presents the parameter settings of the proposed GA–SQP hybrid algorithm for Stage II relay coordination. The GA-based part uses a population of 100 individuals evolved for at most 1000 generations. The top five individuals are kept in each generation to ensure the solutions remain effective. Within the limited TDS search space, a crossover fraction of 0.85, scattered crossover, and adaptive feasible mutation provide an effective balance between exploration and exploitation. The GA starts with the best solutions from 15 multi-start SQP runs, ensuring that the evolutionary search begins in high-quality, feasible areas. The SQP refinement uses step and constraint tolerances of 10^{-8} to ensure accurate results. The analytical lower bounds on TDS_R – *computed* per relay as:

$$TDS_{R,i} \geq TDS_s + \frac{0.35}{K_i} \quad (24)$$

where *R*,*i* is the ratio of the fault current to the relay pickup current, K_i is the relay characteristic and the constant in Equation (24) corresponds to the adopted CTI (0.2 s, or 0.3 s in

the sensitivity case) plus any additional safety margin. The initial individuals are adjusted using this bound so that they satisfy the CTI constraint. The constraint eliminates infeasible evaluations and reduces calculation time compared to penalty-only methods.

For a primary relay p and its backup relay b, the operating time is $t = TDS * K$ with $K = \frac{0.14}{r^{0.02}-1}$, where r is the ratio of the fault current, the relay sees to its pickup current. The coordination constraint $t_b - t_p \geq CTI$ therefore yields $TDS_b \geq \frac{CTI+TDS_p*K_p}{K_b}$. Equation (24) is the particular case $K_p = K_b$; when $K_p \neq K_b$, the general form must be used. For fixed pickup currents, the constraint is linear in the TDS variables.

Table 3. GA–SQP control parameters for Stage II.

Parameter	Value	Algorithm	Description
Population size P_p	100	GA	GA individuals per generation
Max generations G_{max}	1000	GA	GA stopping criterion
Crossover probability P_c	0.85	GA	SBX crossover rate
Mutation probability P_m	Adaptive Feasible	GA	Mutation adapts feasible
Elite fraction	5	GA	Top individuals are preserved each generation
Max stall generation	50	GA	Generations without improvement before stopping
Function tolerance ε	10^{-6}	GA	Convergence threshold
Initial population	SQP-seeds	GA	15 Independent multi-start SQP restarts
Multi-start runs NR_{SQP}	15	SQP	Independent SQP initializations
Max iterations.	1000	SQP	Fmincon maximum iterations
Stop tolerance.	10^{-8}	SQP	Fmincon step size convergence
Total relays	70	GA and SQP	32S + 32R + 6DG (S: sending-end, R: receiving-end and DG: DG-side relays); the main results coordinate the 32 sending-end relays

5. Simulation Results and Discussion

The testing apparatus comprises five normally open tie switches (branches 33–37), each equipped with a switch that can be activated to reconfigure the network as required. The positions of the overcurrent protection devices and faults are illustrated in the distribution network diagram, showing the arrangement of directional relays. The network incorporates five DG units: one synchronous generator, two wind turbines, and two solar PV units. These distributed generation units are integrated to establish an active distribution system, in accordance with the distributed generation placements referenced in the protection coordination literature [3,8,36]. DGs are installed at nodes 17, 18, 25, 29, and 33, as detailed in Table 4, where SCC denotes the short-circuit capacity of the three DG types commonly used in distribution systems.

The proposed method is general and applicable to any protection scheme; however, the following assumptions are made when applying the protection systems to the test system: the capacities of DGs are such that they do not require a complete overhaul of the existing protection schemes within the distribution system. Consequently, traditional protection systems remain applicable. Proposals for new protection schemes or coordination strategies to address various DG conditions are outside the purview of this paper. It is significant that, in a power distribution system, if all protective devices are adaptive, the protection system's

constraints can be overlooked. Upon determining the post-fault topology, the protection devices' settings are subsequently revised. The proposed two-stage method is illustrated in Figure 4.

Table 4. DG specifications in the IEEE 33-bus active distribution system.

DG Unit	Bus	Prated (kW)	Type	Fault Model	SCC (MVA)	X″ (%)
DG1	17	400	Solar PV	Current source, I_{max} = 1.2 pu	0.48	—
DG2	18	400	Solar PV	Current source, I_{max} = 1.2 pu	0.48	—
DG3	25	500	Wind (DFIG)	1 p.u voltage behind X″	2.78	20
DG4	29	350	Synchronous	1 p.u voltage behind X″	3.43	12
DG5	33	500	Wind (DFIG)	1 p.u voltage behind X″	2.78	20

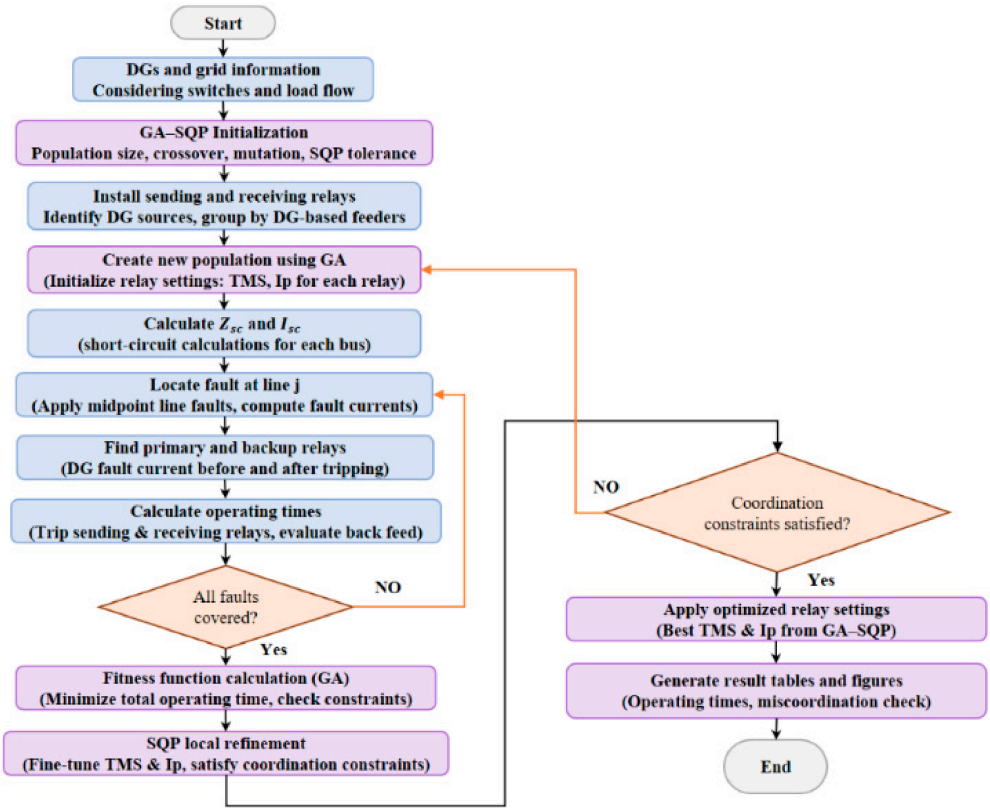


Figure 4. Hybrid flowchart of GA–SQP.

After a faulted segment of the distribution system is isolated by protective devices, DGs are also disconnected through their own islanding mechanisms. As a result, while the fault-current contribution of each DG unit is fully retained in the currents recorded by the substation-fed relays, relays whose fault current is provided only by DG units are not included in the coordination problem addressed in this study.

The proposed framework is validated on the IEEE 33-bus radial distribution system, the most prevalent benchmark for DNR research. The system operates at 12.66 kV with a total nominal load of 3.715 MW active and 2.300 MVAr reactive, supplied by a single substation at bus 1. The fundamental configuration comprises five normally open tie switches (33–37). The initial total active power loss is 202.68 kW, and the minimum bus voltage is 0.9131 pu at bus 18 for the network without DG. With the five DG units in Table 4 connected and

operated at unity power factor, the initial loss is 82.74 kW, and the minimum voltage is 0.9629 pu at bus 31.

For the PV units, the fault current is limited to 1.2 pu of the rated current. X″ is the sub-transient reactance of the rotating machine, which limits the initial short-circuit current. The PV units have no X″.

5.1. Stage I: Reconfiguration Results

5.1.1. Deterministic Case Without DG

The results of the Stage I network reconfiguration under four loading scenarios (100%, 140%, 180%, and 220% of nominal demand) for the deterministic case without distributed generation. Without DG, base-case losses are higher, and voltage drops are more noticeable because all active power is supplied by the main substation at bus 1. This is different from the DG-integrated scenarios. The deterministic HSA is used to reduce active power losses; in these reference cases without DG, the 0.90 pu minimum-voltage limit is not satisfied at 180% and 220% loading, so they serve as loss benchmarks rather than feasible operating points. All simulations were conducted using MATLAB R2023b, while power flow analyses were performed using MATPOWER 7.1. Without DG, the loss-optimal configuration is {7, 9, 14, 32, 37} at all four loading levels. The reconfigured network verifies the implementation's accuracy by achieving a 31.15% loss reduction at 100% loading, matching the benchmark results for the IEEE 33-bus system without DG published in the literature. As the loading increases from 100% to 220%, the loss-reduction percentage increases monotonically, reaching 31.15%, 32.89%, 34.97%, and 37.54% at 140%, 180%, and 220% loading, respectively (Table 5b). This means that network reconfiguration works better at higher loading, where resistive losses are most noticeable. At 180% and 220% loading, the minimum voltage of the reconfigured network (0.8822 and 0.8517 pu) remains below 0.90 pu even in the loss-optimal configuration. The absence of DG injections eliminates bidirectional fault-current contributions that hinder protection coordination in active networks, establishing a clean baseline for comparing DG-integrated scenarios. These results show that performance improvement is due solely to network reconfiguration, not DG. They also serve as a baseline for measuring the extra benefit of DG integration in later scenarios.

Table 5. (**a**) Stage I reconfiguration results—base case without DG (nominal loading). (**b**) (continued). Loss-optimal configuration.

(**a**)

Method	Open SW	P_{loss} (kW)	V_{min} (pu)	Loss Red. (%)	Reference
Initial Config.	33,34,35,36,37	202.68	0.9131	—	—
GA	7,9,14,28,32	139.98	0.9413	30.93	[37]
PSO	7,9,14,32,37	139.55	0.9375	31.15	[38]
Cuckoo Search	7,9,14,32,37	139.55	0.9375	31.15	[39]
Firefly Algorithm	7,9,14,32,37	139.55	0.9375	31.15	[40]
MILP	7,9,14,32,37	139.55	0.9375	31.15	[41]
Proposed HSA	7,9,14,32,37	139.55	0.9378	31.15	Proposed

Table 5. *Cont.*

(**b**)					
Load (%)	**Initial Loss (kW)**	**Optimal Loss (kW)**	**Loss Red. (%)**	**V_{min}, Initial (pu)**	**V_{min}, Optimal (pu)**
100	202.68	139.55	31.15	0.9131	0.9378
140	424.65	285.00	32.89	0.8738	0.9108
180	757.42	492.55	34.97	0.8308	0.8822
220	1236.67	772.37	37.54	0.7829	0.8517

For the IEEE 33-bus system without DG, with an initial configuration that has a base loss of 202.68 kW and a minimum voltage of 0.9131 pu, Table 5 compares the suggested deterministic HSA with five tried-and-true optimization methods. The recommended HSA converges with the ideal open-switch configuration {7, 9, 14, 32, 37} with a power loss of 139.55 kW, a minimum voltage of 0.9378 pu, and a loss reduction of 31.15%. The results are exactly what PSO [38], Cuckoo Search [39], Firefly Algorithm [40], and MILP [41] found, and they all point to the same best topology. The HSA reproduced this configuration in repeated runs with different random seeds. The proposed method outperforms the GA benchmark [37], which yields a sub-optimal configuration {7, 9, 14, 28, 32} with a lower loss reduction of 30.93% and a higher loss of 139.98 kW. This shows that HSA performs better than GA in searching the combinatorial space of switch configurations. The exact replication of the globally optimal solution, independently verified by four optimization paradigms (metaheuristics, swarm intelligence, and exact mathematical programming), provides strong evidence that the proposed HSA is optimal and correct. This result can serve as a better benchmark for the additional performance improvements achieved by protection coordination and the integration of distributed generation in the subsequent stages of the proposed two-stage framework.

5.1.2. Active Distribution System with DG

The IEEE 33-bus system's Stage I results at nominal loading, with the five DG units from Table 4 all running at unity power factor, are shown in Table 6. The initial arrangement, with tie switches 33–37 open, has a minimum bus voltage of 0.9629 pu at bus 31 and a loss of 82.74 kW when the DG units are connected. The suggested HSA converges to the open-switch configuration {7, 10, 12, 28, 36}, which increases the minimum voltage to 0.9727 pu and lowers the loss to 65.02 kW (a reduction of 21.42%). This set is the best configuration found for the loss objective, and the HSA reached it at each iteration across various random seeds. The configurations reported in the literature for the network without DG [37,41], and the Firefly Algorithm configuration given in [13] were reevaluated on the current test system to determine the impact of the DG units on the reconfiguration problem. These combinations result in losses that are 25.6–33.9% greater than the original setup, or 103.94–110.79 kW. Therefore, once the DG units are coupled, a topology that is ideal without DG may become noticeably sub-optimal or even harmful. (The Evolutionary Programming (EP) configuration {11, 31, 33, 36, 37} described in [13] was not analyzed because it is not radial in the current network.

Table 6. Stage I reconfiguration results—IEEE 33-bus with DG.

Method	Open SW	P_{loss} (kW)	V_{min} (pu)	Change vs. Initial (%)
Initial configuration + DG	33,34,35,36,37	82.74	0.9629	—
Configuration of [37,41] (optimal without DG)	7,9,14,32,37	110.79	0.9513	+33.90
Configuration of GA [37]	7,9,14,28,32	105.41	0.9595	+27.40
Configuration of FA [13]	11,13,32,33,37	103.94	0.9538	+25.62
Proposed HSA + DG	7,10,12,28,36	65.02	0.9727	−21.42

5.1.3. Active Distribution System—4 Load Scenarios with DG

The Stage I findings for the four loading levels (100%, 140%, 180%, and 220% of nominal demand) are compiled in Table 7. With loading, the DG-connected network's initial losses rise from 82.74 kW to 668.80 kW; the HSA lowers these losses to 65.02, 137.10, 259.61, and 442.21 kW, representing reductions of 21.42%, 28.24%, 31.70%, and 33.88%, respectively (Figure 5). Because the resistive losses give a greater margin for improvement and expand with the square of the branch currents, the loss reduction consequently grows monotonically with the loading. Additionally, reconfiguration enhances the voltage profile at all loading levels: the minimum voltage increases from 0.9629 to 0.9727 p.u. at 100%, from 0.9291 to 0.9542 p.u. at 140%, from 0.8927 to 0.9167 p.u. at 180%, and from 0.8531 to 0.9064 p.u. at 220%. Therefore, in all four instances, the reconfigured network meets a 0.90 p.u. lower-voltage limit, while the original configuration exceeds it at 180% and 220% loads. The appropriate open-switch configuration varies with load: {7, 10, 12, 28, 36} at 100%, {7, 10, 14, 28, 30} between 140% and 180%, and {7, 10, 14, 28, 31} at 220%. The final solution is the best configuration found for the loss objective subject to the voltage restriction, and it was consistently obtained across repeated runs with different random seeds. However, the harmony search by itself stopped 1.6% and 1.5% over the ultimate cost at 180% and 220% loading, respectively, and the final single-switch exchange (branch-exchange refinement) applied to the best harmony filled this gap. Lastly, when compared to the network without DG, the DG units lower the initial loss by 59.2% at 100% loading (202.68 to 82.74 kW) and by 45.9% at 220% loading (1236.67 to 668.80 kW).

Table 7. HSA reconfiguration results—4 load scenarios.

Load (%)	Open SW	Initial Loss (kW)	Loss (kW)	Loss Red (%)	V_{min}, Initial (pu)	V_{min}, Optimal (pu)
100	7,10,12,28,36	82.74	65.02	21.42	0.9629	0.9727
140	7,10,14,28,30	191.04	137.10	28.24	0.9291	0.9542
180	7,10,14,28,30	380.08	259.61	31.70	0.8927	0.9167
220	7,10,14,28,31	668.80	442.21	33.88	0.8531	0.9064
100	7,10,12,28,36	82.74	65.02	21.42	0.9629	0.9727

Figure 6 illustrates how the reconfiguration affected the voltage profile. Every bus in both configurations has a voltage within 0.95 pu at 100% loading, and the reconfiguration increases the minimum from 0.9629 to 0.9727 pu. The number of buses below 0.95 pu decreases from 17 to zero at 140% loading, from 21 to 17 and from 23 to 19 at 180% and 220% loading, respectively, and from 4 to zero and from 17 to zero at 0.90 pu. The portion of the feeder that is furthest from the substation, the end of the lateral between buses 26 and 33, is the weakest area of the network.

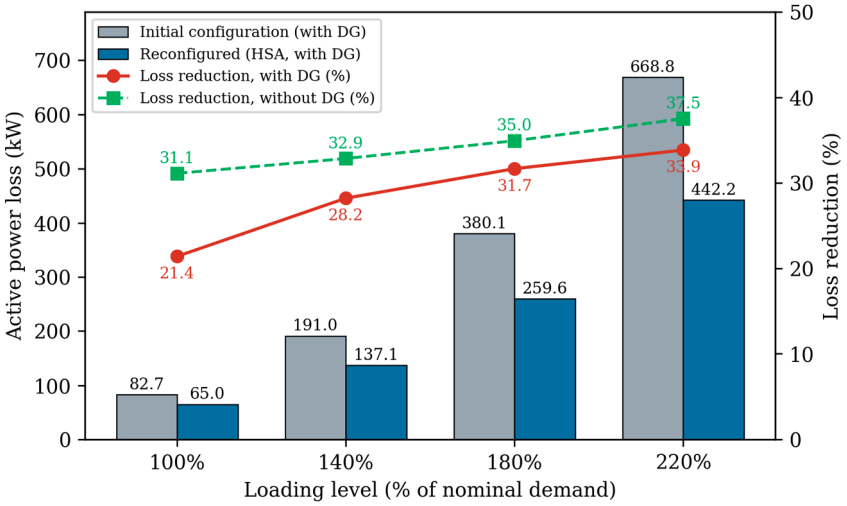


Figure 5. Active power loss before and after reconfiguration and loss reduction.

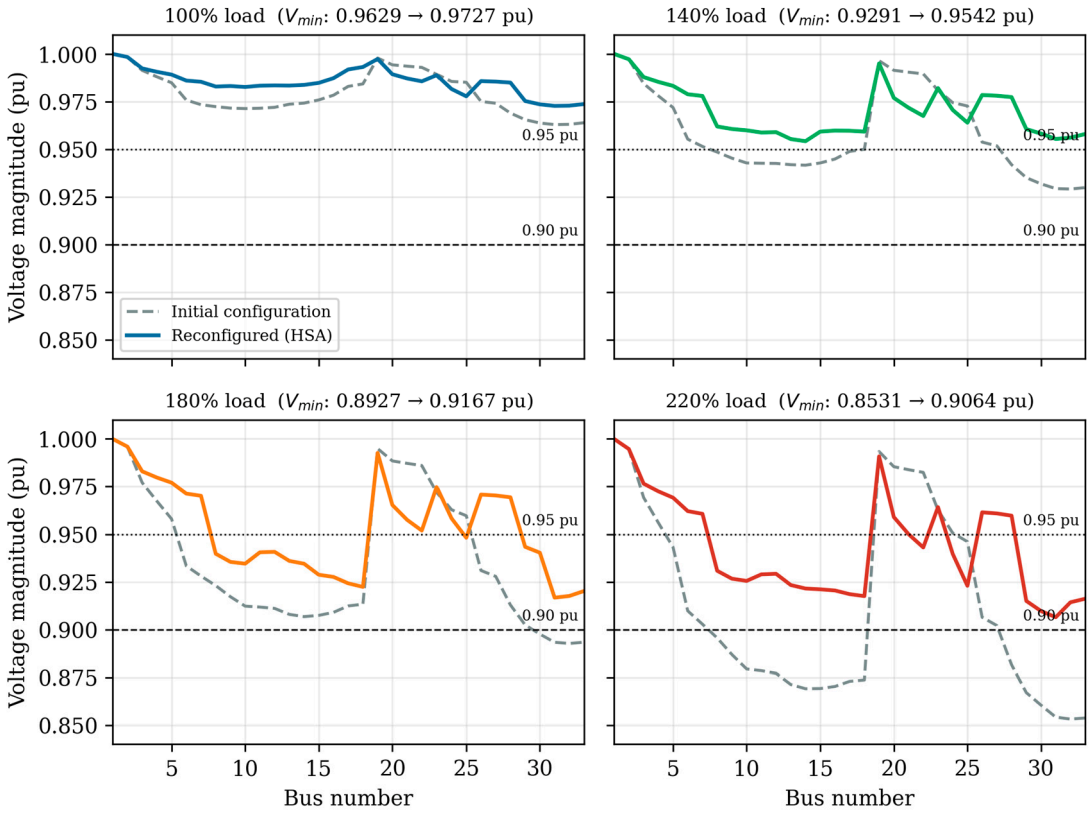


Figure 6. Bus voltage profiles of the initial and the reconfigured network at the four loading levels.

Figure 7 illustrates the HSA's convergence. As better switch combinations reach the harmony memory, the best cost, which is calculated by dividing the loss by the initial loss plus the voltage-violation penalty, gradually drops. In the run described here, the harmony search's last improvement happens after 1845, 1575, 1074, and 584 iterations at 100%, 140%, 180%, and 220% loading, respectively. The search is terminated after 600 iterations without improvement. As shown above, the refining phase maintains the previous two options while reducing the final cost by 1.6% and 1.5% at 180% and 220% loading. While the final results were the same in repeated runs, the number of iterations depends on the random sequence.

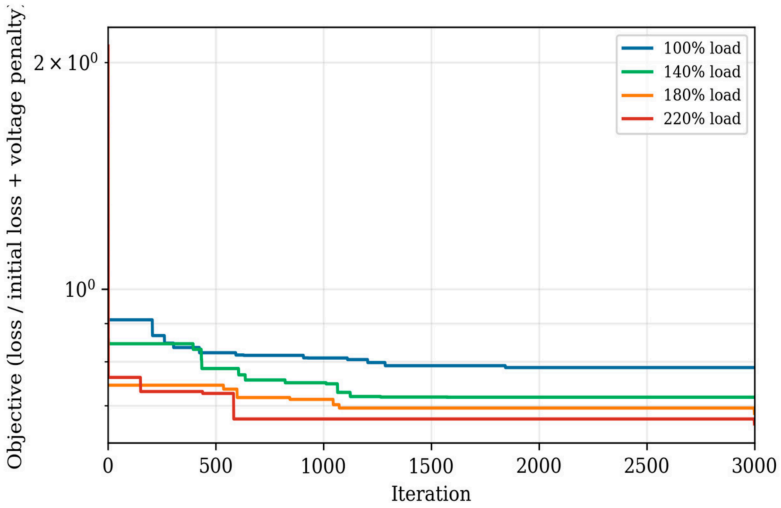


Figure 7. Convergence of the harmony search algorithm for the four loading levels.

5.2. Stage II: Relay Coordination Results

This section examines the coordination outcomes of primary and backup relays when fault current traverses them from various directions. The relay's performance is influenced by the fault type (e.g., phase-phase or phase-to-ground) and the fault resistance. These uncertainties can modify the magnitude without affecting the fault direction. Consequently, this study assumes a three-phase bolted fault current at the midpoint of the lines on the 33-Bus radial distribution network.

Coordination model. Each protected line is equipped with two directional overcurrent relays, one at each end, and each relay responds only to the current flowing into its own end of the line. The operating time follows the IEC standard inverse characteristic of Equation (2), $t = \frac{14}{R^{0.02}-1}\ TDS$, where $R = I_f/I_p$ is the ratio of the fault current, the relay sees to its pickup current. The pickup current is set to 1.25 times the largest load current of the protected line, evaluated for two operating states (all DG units in service and all DG units out of service), rounded to the nearest 5 A, with a minimum of 10 A. The pickup currents are therefore fixed inputs, and the TDS values are the only decision variables in Stage II. A relay is regarded as sensing a fault only if R ≥ 1.5. The fault currents are derived from a positive-sequence short-circuit analysis of the modified network, in which the substation is modeled as 1 p.u. voltage source with a backing of 0.1 p.u. (100 MVA short-circuit capacity), the DFIG and synchronous units as 1-pu voltage sources behind their sub-transient reactance (refer to Table 4), the PV units as constant-current sources capped at 1.2 pu of their rated current, and the loads are disregarded (Table 8). The primary–backup pairs are automatically determined from the network configuration: in the event of a fault on the line k (k = line number), the primary relays are those situated at both extremities of line k, while the backup relay for the primary relay at bus u is the relay at the opposite end of any other closed line linked to u that is oriented toward u (u = *bus number*).

The primary–backup pairs are automatically identified for the radial configuration returned by Stage I as follows. (1) The closed branches are assembled into a graph, and a breadth-first search from the substation bus yields the upstream–downstream ordering of the lines. (2) For each protected line k = (u, v), the two relays at its ends act as primary relays. (3) The backup relays of the primary relay at bus u are the relays at the far ends of every other closed line connected to u that is oriented toward u, and likewise for bus v. (4) A pair is retained only if the backup relay senses the fault (R ≥ 1.5), with the DG contributions included through the short-circuit analysis. (5) Relays supplied solely by DG units are excluded from the main coordination.

Table 8. Fault-study and relay-model parameters used in Stage II.

Load (%)	V_{min}, Optimal (pu)
Fault	Three-phase bolted fault at the midpoint of every closed line
Substation	1 pu voltage source behind 0.1 pu on the 10 MVA base (100 MVA short-circuit capacity)
Solar PV units	Constant current source, 1.2 p.u of rated current
DFIG and synchronous units	1 pu voltage source behind the sub-transient reactance X″ of Table 4
Loads	Neglected during the fault
Relays	Directional overcurrent relays at both ends of each line; IEC standard inverse (0.14, 0.02)
Pickup current	1.25 × largest line load current (DG in and out of service), rounded to 5 A, minimum 10 A
Sensing condition	$I_f/I_p \geq 1.5$
TDS limits	$0.05 \leq \text{TDS} \leq 1.0$
Coordination time interval	CTI = 0.2 s (0.3 s as sensitivity case)
Coordinated relays	Relays fed by the substation (DG units assumed to be disconnected by their islanding protection)
Solver	Linear programming (global optimum)

Optimization problem: The coordination problem is formulated as the minimization of the total operating time of the primary relays, $\sum t_p$, subject to the coordination constraint $t_b - t_p \geq CTI$ for every primary–backup pair and to $0.05 \leq TDS \leq 1.0$. A CTI of 0.2 s is adopted, as in [26,42]; it comprises the circuit-breaker opening time, the relay overtravel, and a safety margin [26], and a CTI of 0.3 s is also examined as a sensitivity case. Stage II is addressed using the hybrid GA–SQP algorithm: a real-coded GA (with a population of 100 and a maximum of 1000 generations) minimizes the total primary operating times while imposing a penalty for CTI violations (Equation (23)), and the optimal individual then initiates an SQP refinement of the constrained problem. Ten autonomous trials, each using a distinct random seed, were conducted for each scenario. Due to the linearity of the TDS values, the global optimum can be precisely determined by linear programming, and this value serves as an independent benchmark. Across all 80 iterations (comprising four loading levels, two CTI values, and ten seeds), the GA–SQP achieved the benchmark optimum (gap 0.0000%, standard deviation 0 s throughout the runs), but the GA alone fell short by 7–12%; hence, the SQP phase is crucial for precise CTI fulfillment and optimality. Since the problem is linear for fixed pickup currents, linear programming solves it exactly. The GA–SQP is retained as a general-purpose solver, applicable when pickup or discrete settings are also optimized, and its results are reported against the LP optimum.

The coordination outcomes for the ideal architecture at each loading level are encapsulated in Table 9. In each of the four scenarios, the 32 synchronized relays and the 31 primary–backup pairs adhere to the coordination requirement with no CTI infractions, and the minimum CTI is precisely 0.2 s; this constraint is applicable in 25 out of the 31 pairs, while in the other pairs, the backup relay, which is also responsible for supporting another primary relay, possesses a greater margin. The aggregate primary operational durations are 18.40 s at full capacity, 19.47 s at 140%, 19.04 s at 180%, and 18.14 s at 220%, yielding average operating times of 0.57–0.61 s per relay and a peak individual duration of 1.19–1.36 s (Figures 9–12). The overall amount is largely unaffected by the load, consistent with the

scaling of pickup currents relative to branch currents, resulting in very slight variations in the ratios of fault to pickup currents. The pickup currents vary from 10 A to 260 A, 375 A, 490 A, and 605 A at loading levels of 100%, 140%, 180%, and 220%, with the peak values associated with the relays at the feeder head, while the maximum TDS is recorded at 0.65, 0.59, 0.53, and 0.50, far under the upper limit of 1.0. The relays nearest to the substation are the slowest, as they must operate at a slower speed than all downstream relays they support; this is a fundamental result of time grading in a radial feeder. With a CTI of 0.3 s, the total principal operational durations are 26.43, 28.08, 27.38, and 26.01 s, with no infractions in any instance. When the relays powered solely by the DG units are incorporated into the coordination (CTI = 0.2 s), the count of active primary relays increases to 41, 42, 39, and 37. At the same time, the total duration increases to 34.91, 31.75, 26.32, and 22.95 s. Under nominal loads, the nine distributed generation-fed relays contribute 16.5 s, with operational durations reaching 2.54 s, since their fault currents (about 125 A) are near the pickup thresholds and the relays establish extensive coordination chains; also, 11 to 14 pairs lack a backup relay to detect the fault. This supports the premise that distributed generation units are isolated by their own safeguards following the fault.

Table 9. Stage II coordination results for the optimal topology at each loading level (32 coordinated relays unless otherwise stated).

Load (%)	Case	Primary Relays	Pairs	$\sum t_p$ (s)	Mean t_p (s)	Max t_p (s)	Min CTI (s)	CTI Viol	Max TDS	Pickup (A)
100	Proposed, CTI = 0.2 s	32	31	18.40	0.57	1.35	0.200	0	0.65	10–260
	CTI = 0.3 s	32	31	26.43	0.83	2.00	0.300	0	0.95	10–260
	With DG-fed relays, CTI = 0.2 s	41	41	34.91	0.85	2.54	0.200	0	0.65	10–260
140	Proposed, CTI = 0.2 s	32	31	19.47	0.61	1.36	0.200	0	0.59	10–375
	CTI = 0.3 s	32	31	28.08	0.88	2.01	0.300	0	0.87	10–375
	With DG-fed relays, CTI = 0.2 s	42	41	31.75	0.76	1.65	0.200	0	0.59	10–375
180	Proposed, CTI = 0.2 s	32	31	19.04	0.59	1.27	0.200	0	0.53	10–490
	CTI = 0.3 s	32	31	27.38	0.86	1.88	0.300	0	0.78	10–490
	With DG-fed relays, CTI = 0.2 s	39	36	26.32	0.67	1.35	0.200	0	0.53	10–490
220	Proposed, CTI = 0.2 s	32	31	18.14	0.57	1.19	0.200	0	0.50	10–605
	CTI = 0.3 s	32	31	26.01	0.81	1.76	0.300	0	0.74	10–605
	With DG-fed relays, CTI = 0.2 s	37	34	22.95	0.62	1.27	0.200	0	0.50	10–605

5.2.1. Protection System for Optimal Topology

For Stage I, as illustrated in Table 7, the ideal topology for all four scenario sets is achieved, and the previously outlined automatic relay identification method establishes the primary–backup pairings for each topology; the resulting coordination is encapsulated in Table 9.

The ideal configurations for the four loading tiers are illustrated in Figure 8. The switches S7, S10, and S28 remain open across all loading levels; moreover, switches S12 and S36 are open at 100% loading, S14 and S30 at 140% and 180% loading, and S14 and S31 at 220% loading. The tie lines S33, S34, S35, and S37 are inactive in every scenario. The DG units are linked to buses 17, 18, 25, 29, and 33 across all situations.

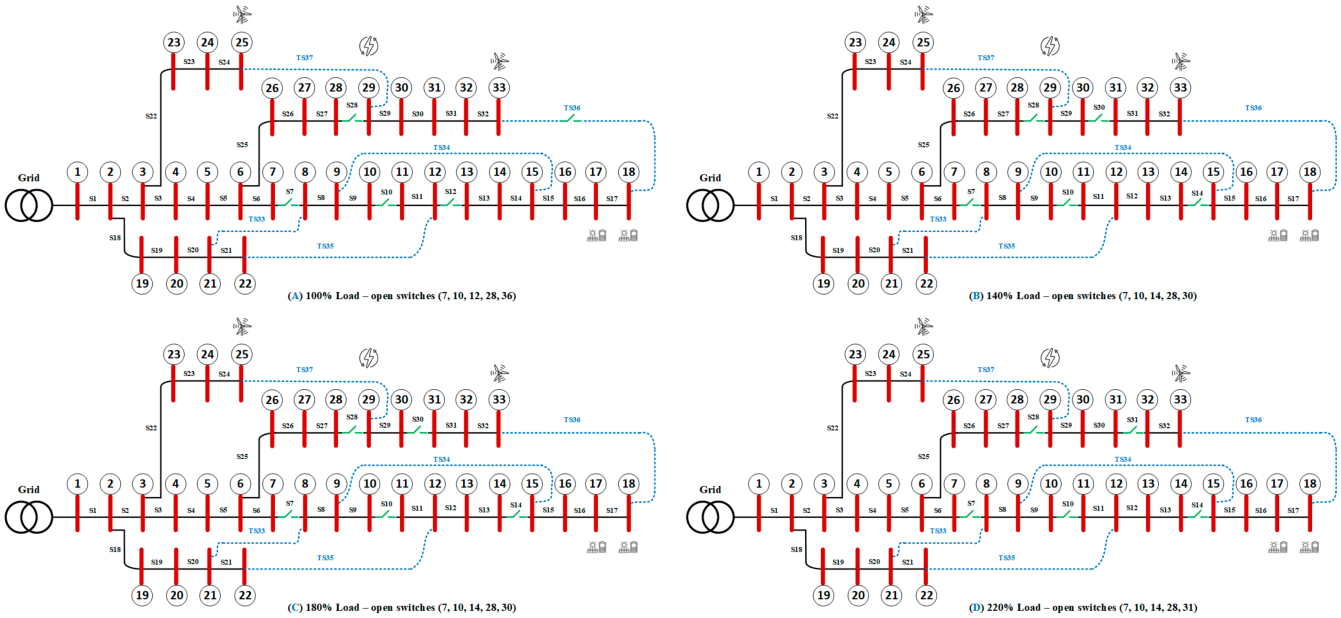


Figure 8. IEEE 33-bus network with the optimal open switches at (**A**) 100%, (**B**) 140%, (**C**) 180%, and (**D**) 220% loading, the closed tie lines, and the DG locations.

5.2.2. Optimization Relay Settings and CTI Robustness

The ideal relay configurations for the 32 coordinated relays are presented in Table 10 across four loading levels, arranged according to the protected line number; each relay is designated by the line it safeguards and its terminal (S: sending end, R: receiving end), and a line that is unoccupied at a specific loading level lacks a relay. The pickup currents, established at 1.25 times the maximum line current, vary from 10 A for the minimally loaded laterals to 260, 375, 490, and 605 A at the feeder head (relay 1.S) under 100%, 140%, 180%, and 220% loading, respectively, indicating a correlation with the loading, while the fault currents detected by the relays span from 506 A to 4527 A. The TDS values fluctuate from a minimum of 0.05 for the most distant relays to 0.647, 0.586, 0.533, and 0.503 across four loading levels, remaining significantly below the maximum threshold of 1.0, resulting in primary operating times ranging from 0.07 s to 1.35, 1.36, 1.27, and 1.19 s, while backup operating times span from 0.27 s to 1.41, 1.42, 1.33, and 1.26 s, respectively. All 31 primary–backup pairs are synchronized at each loading level, exhibiting CTIs ranging from 0.200 s to 0.734, 1.156, 1.129, and 1.007 s. The CTI constraint is engaged in 25 out of 31 pairs at every loading level; in the remaining pairs, the backup relay also serves as a backup for a second primary relay, with the more stringent of the two pairs dictating its configuration, allowing a greater margin for the other.

Figure 9 consolidates the main operational durations of all synchronized relays across the four loading tiers into a single chart. The profiles exhibit notable similarity: the timings diminish consistently along the primary feeder, ranging from 1.19 to 1.36 s at the feeder-head relay 1.S to 0.62 s at relay 5.S, since each relay must work at a slower pace than those it supports, while the relays at the extremities of the laterals function in approximately 0.07 s. The most extended durations (1.0–1.2 s) pertain to relays 8.S, 18.S–20.S, and 33.S–34.S, which dominate the network's branches. The relay configuration varies marginally across loading levels due to the differing open switches (S12 and S36 are open exclusively at 100%, whereas S14 and S30 are open at 140% and 180%, respectively). The quantity of relays exhibiting an operational duration of no more than 0.5 s is 16, 15, 15, and 14 out of 32 relays, while 26, 24, 24, and 26 relays function within 1.0 s or less under 100%, 140%, 180%, and 220% loading, respectively.

Table 10. Optimal relay settings of the coordinated relays for the four loading levels.

Line	100% Relay	Pickup (A)	TDS	tp (s)	140% Relay	Pickup (A)	TDS	tp (s)	180% Relay	Pickup (A)	TDS	tp (s)	220% Relay	Pickup (A)	TDS	tp (s)
1	1.S	260	0.567	1.353	1.S	375	0.493	1.355	1.S	490	0.410	1.268	1.S	605	0.347	1.188
2	2.S	175	0.559	1.207	2.S	205	0.469	1.060	2.S	265	0.422	1.046	2.S	355	0.371	1.031
3	3.S	40	0.635	0.937	3.S	55	0.582	0.928	3.S	75	0.533	0.919	3.S	90	0.503	0.913
4	4.S	30	0.539	0.771	4.S	45	0.485	0.765	4.S	60	0.448	0.759	4.S	70	0.427	0.754
5	5.S	30	0.408	0.620	5.S	40	0.378	0.618	5.S	50	0.355	0.615	5.S	65	0.329	0.612
6	6.S	15	0.050	0.069	6.S	20	0.050	0.073	6.S	25	0.050	0.077	6.S	30	0.050	0.081
7	open	—	—	—	open	—	—	—	open	—	—	—	open	—	—	—
8	8.S	35	0.378	0.770	8.S	80	0.420	1.149	8.S	110	0.353	1.112	8.S	110	0.317	0.999
9	9.S	10	0.050	0.075	9.S	10	0.050	0.074	9.S	10	0.050	0.074	9.S	10	0.050	0.074
10	open	—	—	—	open	—	—	—	open	—	—	—	open	—	—	—
11	11.R	10	0.050	0.074	11.R	10	0.050	0.074	11.R	10	0.050	0.074	11.R	10	0.050	0.074
12	open	—	—	—	12.S	20	0.148	0.267	12.S	25	0.143	0.275	12.S	30	0.138	0.281
13	13.R	10	0.050	0.081	13.S	10	0.050	0.078	13.S	15	0.050	0.087	13.S	20	0.050	0.094
14	14.R	15	0.156	0.276	open	—	—	—	open	—	—	—	open	—	—	—
15	15.S	35	0.201	0.470	15.S	65	0.321	0.961	15.S	85	0.280	0.951	15.S	80	0.246	0.810
16	16.S	35	0.119	0.291	16.S	60	0.268	0.818	16.S	80	0.232	0.816	16.S	70	0.202	0.663
17	17.S	20	0.050	0.104	17.S	55	0.217	0.662	17.S	70	0.195	0.666	17.S	60	0.158	0.502
18	18.S	80	0.647	1.077	18.S	160	0.586	1.194	18.S	215	0.495	1.109	18.S	240	0.442	1.030
19	19.S	75	0.551	1.022	19.S	155	0.508	1.191	19.S	205	0.427	1.112	19.S	225	0.380	1.027
20	20.S	70	0.465	0.953	20.S	145	0.446	1.183	20.S	195	0.370	1.113	20.S	215	0.325	1.021

Table 10. *Cont.*

Line	100% Relay	Pickup (A)	TDS	tp (s)	140% Relay	Pickup (A)	TDS	tp (s)	180% Relay	Pickup (A)	TDS	tp (s)	220% Relay	Pickup (A)	TDS	tp (s)
21	21.S	15	0.296	0.425	21.S	35	0.323	0.566	21.S	50	0.290	0.563	21.S	60	0.275	0.563
22	22.S	130	0.522	1.092	22.S	140	0.331	0.707	22.S	185	0.297	0.696	22.S	255	0.292	0.773
23	23.S	120	0.447	1.004	23.S	135	0.250	0.582	23.S	175	0.225	0.578	23.S	240	0.232	0.676
24	24.S	95	0.400	0.923	24.S	95	0.198	0.455	24.S	125	0.180	0.458	24.S	180	0.198	0.584
25	25.S	10	0.360	0.449	25.S	15	0.330	0.449	25.S	20	0.309	0.448	25.S	25	0.293	0.447
26	26.S	10	0.202	0.255	26.S	10	0.202	0.255	26.S	15	0.185	0.255	26.S	15	0.185	0.255
27	27.S	10	0.050	0.066	27.S	10	0.050	0.066	27.S	10	0.050	0.066	27.S	10	0.050	0.066
28	open	—	—	—	open	—	—	—	open	—	—	—	open	—	—	—
29	29.S	60	0.299	0.628	29.S	55	0.050	0.102	29.S	70	0.050	0.111	29.S	105	0.104	0.266
30	30.S	30	0.258	0.465	open	—	—	—	open	—	—	—	30.S	25	0.050	0.086
31	31.S	20	0.170	0.285	31.R	15	0.050	0.094	31.R	20	0.050	0.102	open	—	—	—
32	32.S	25	0.050	0.091	32.R	35	0.119	0.289	32.R	50	0.106	0.297	32.R	35	0.050	0.121
33	33.S	50	0.424	0.876	33.S	100	0.448	1.184	33.S	135	0.377	1.131	33.S	140	0.338	1.031
34	34.S	30	0.302	0.632	34.S	70	0.375	1.073	34.S	95	0.320	1.051	34.S	90	0.289	0.924
35	35.R	10	0.184	0.262	35.R	30	0.230	0.427	35.R	40	0.213	0.430	35.R	45	0.207	0.434
36	open	—	—	—	36.S	45	0.170	0.479	36.S	60	0.151	0.486	36.S	45	0.112	0.315
37	37.S	70	0.364	0.794	37.S	65	0.136	0.290	37.S	85	0.127	0.297	37.S	125	0.164	0.443
Σ tp				18.40				19.47				19.04				18.14

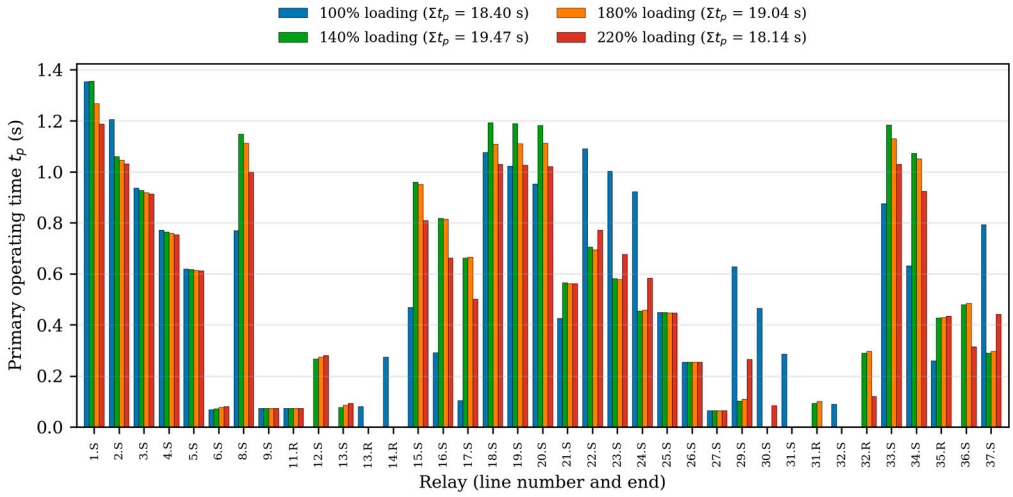


Figure 9. Primary operating times of the coordinated relays.

The synchronization time intervals for all primary–backup pairings are illustrated in Figure 10. In every loading situation, 25 out of the 31 pairs precisely meet the designated CTI of 0.2 s, with the lowest being 0.200 s, ensuring no pair is breached. The last six pairings exhibit greater intervals, with maximums of 0.73, 1.16, 1.13, and 1.01 s at 100%, 140%, 180%, and 220% loading, respectively. These pairs consist of a backup relay whose configuration is dictated by a secondary, more stringent primary relay; hence, their increased margin results from the coordination of the other pair rather than an excessive coordination of the pair in question.

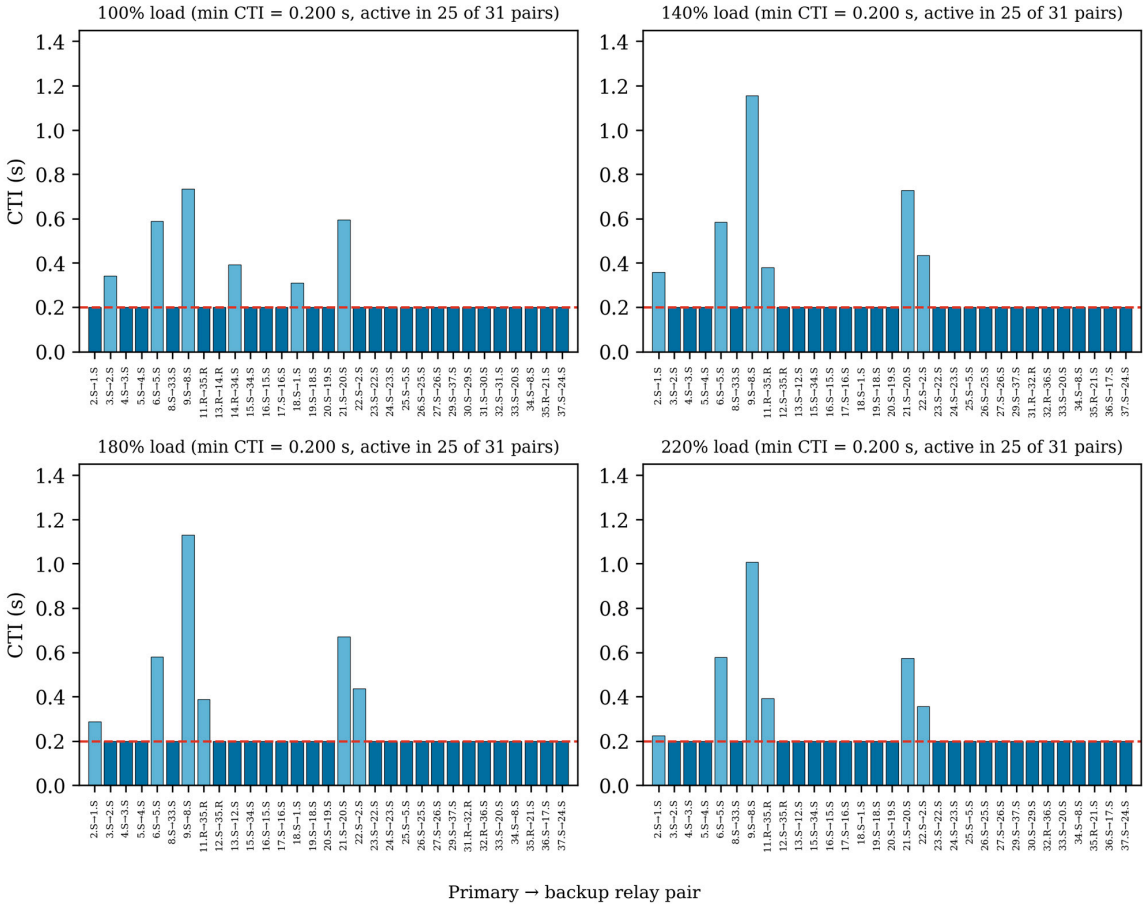


Figure 10. Coordination time interval.

The time current profiles of the five relays at the main feeder's head are illustrated in Figure 11 for the four loading conditions. The main operating points (filled circles) and the alternative operating points for the identical fault (open circles) are situated on the characteristics of the corresponding relays, and these characteristics do not intersect within the fault current range of the feeder, thereby validating the appropriate grading of the relays; as the load intensifies, the characteristics shift to elevated pickup currents and diminished TDS values (the pickup of relay 1.S is 260, 375, 490, 605 A at the four loading levels). The duration between the backup and the primary operational periods is precisely 0.200 s for the 4.S–3.S and 5.S–4.S across all loading tiers, for the 3.S–2.S duo at 140%, 180%, and 220% loadings, as well as for the pair, two seconds to one second at full capacity. The anomalies consist of the duo 3.S–2.S at full capacity (0.343 s) and the combination 2.S–1.S at 140%, 180%, and 220% capacity (0.358, 0.289, and 0.226 s). In these instances, the backup relay (relay 2.S at full capacity, relay 1.S at varying load levels) serves as the backup for an additional primary relay (relays 22.S and 18.S, respectively), with the second pair's interval precisely 0.200 s dictating its configuration.

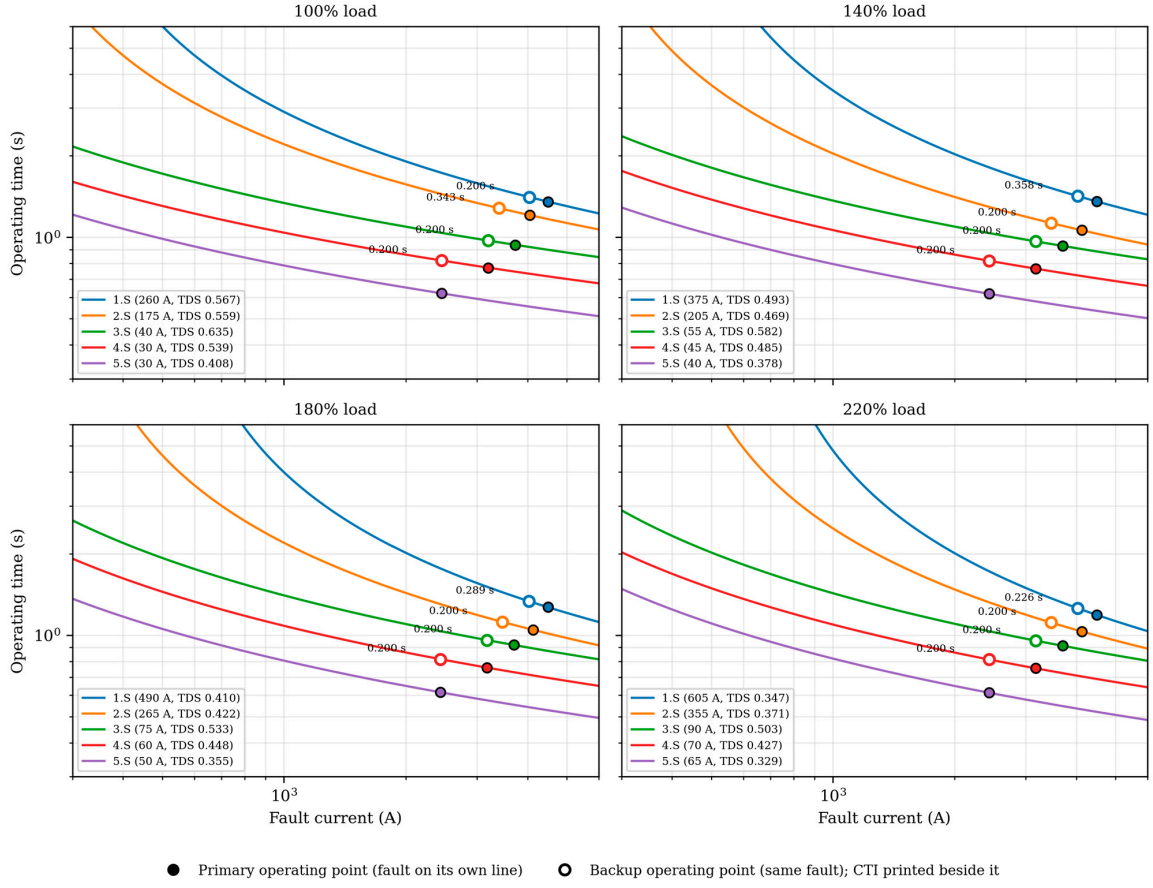


Figure 11. Time–current characteristics of the relays 1.S–5.S.

Ultimately, Figure 12 illustrates the correlation between the entire primary operating duration and both the loading level and the coordination time interval. The overall duration is mostly unaffected by the loading, ranging from 18.14 to 19.47 s for CTI = 0.2 s and from 26.01 to 28.08 s for CTI = 0.3 s. For a certain load, it escalates linearly with the CTI, at a pace of 79 to 86 s per second of CTI, due to the active coordination requirements of the relay chains across most pairings; for instance, at full load, the total is 10.36 s for CTI = 0.1 s and 26.43 s for CTI = 0.3 s. With a TDS cap of 1.0, viable configurations permit CTI values of 0.30 s at 100% and 140% loads, 0.35 s at 180% load, and 0.40 s at 220% load; extended intervals require TDS values exceeding 1.0 (shown by dotted lines).

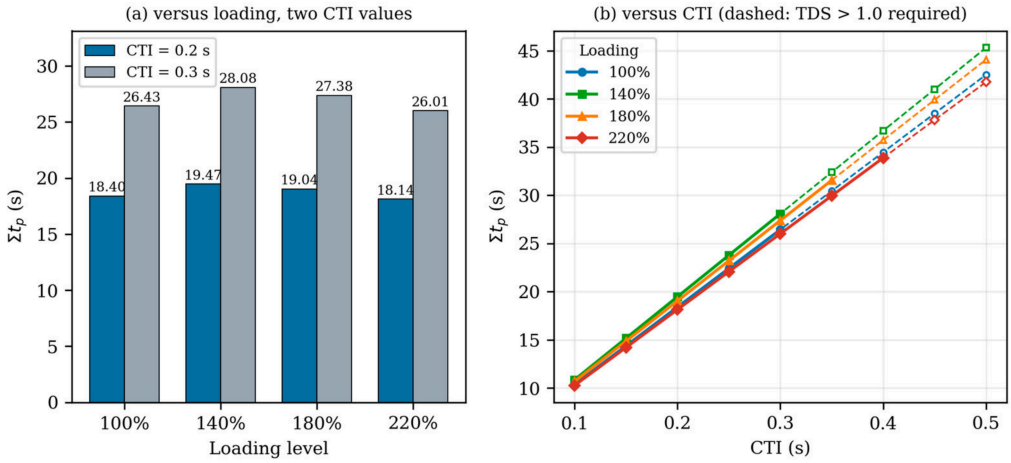


Figure 12. Sum of the primary operating times: (**a**) versus loading level for CTI = 0.2 s and 0.3 s; (**b**) versus CTI for the four loading levels.

The proposed framework for overcurrent relay coordination in distribution networks integrated with distributed generation is compared to four benchmark methodologies in Table 11. Due to variations in size and protective coverage among the benchmark systems, a direct comparison of overall primary operating times is only meaningful when adjusted for the number of coordinated relays; thus, the per-relay metric serves as a relevant, size-agnostic indicator. Under standard loading conditions, the suggested framework achieves a cumulative primary operating duration of 18.40 s across 32 synchronized relays, equating to 0.575 s per relay, while maintaining the identical CTI of 0.2 s as established in the reference studies. This figure is inferior to the measurements recorded by [43] (1.332 s/relay) and [31] (3.713 s/relay), although superior to that of [36] (0.310 s/relay). The benchmarks pertain to various networks, fault sites, and protection ranges (the suggested framework only addresses relays supplied by substations, assuming that distributed generation units cease operation post-fault); thus, the comparison should be viewed as suggestive. Accordingly, no superiority over the published methods is claimed; the like-for-like comparison is between GA, GA–SQP, and the exact LP optimum on the same network and constraints (Section 5 and Table 12). The proposed framework, in addition to the per-relay operating time, (i) integrates network reconfiguration with protection coordination, (ii) is assessed at four distinct loading levels ranging from 100% to 220%, while benchmarks utilize a singular level, and (iii) produces globally optimal solutions devoid of CTI violations: the network configuration identified by the Harmony Search Algorithm in Stage I was reproduced in repeated runs with different random seeds, and the relay settings determined by the hybrid GA–SQP in Stage II consistently align, across ten independent trials, with the precise linear-programming optimum.

The data for the hybrid GA–SQP are presented in Table 12. After 1000 generations, the Genetic Algorithm remains 7–12% superior to the optimum, with certain individuals breaching the CTI constraints, while the Sequential Quadratic Programming refinement, initiated from the top GA individual, took around 5 s to compute per execution. Table 12 therefore provides the comparison under identical conditions (same network, loading levels, pickup currents and CTI): GA alone ends 7–12% above the exact optimum (for example 19.88 s versus 18.40 s at 100% loading and CTI = 0.2 s), with some individuals violating the CTI constraint; the GA–SQP reaches the exact linear-programming optimum in all ten runs (standard deviation 0 s, 10/10 feasible runs, no CTI violation); and the multi-start SQP runs converge to the same objective value, as expected from the linear structure of the problem. The additional computation time of the SQP refinement is about 5 s per run.

Table 11. Optimization methods for OCR coordination.

Criterion	Shrivastava et al. [44]	El-Sayed & Elattar [43]	Al-Bhadeley & Inan [36]	Reiz et al. [31]	Proposed
Algorithm	GWO	HHO-SQP hybrid	HHO-SQP hybrid	GA	Hybrid GA–SQP
Test system	IEEE 33-bus	IEEE 30-bus	IEEE 30-bus	IEEE 33-bus	IEEE 33-bus
No. of relays	32	38	42	8	32
Year	2021	2021	2023	2024	This work
Total t_p (s)	N/A	50.609	13.017	29.700	18.397 (100% load)
t_p/relay (s)	N/A	1.332	0.310	3.713	0.575
CTI (s)	0.20	0.20	0.20	~0.20	0.20 (0.30 sensitivity)
Loading scenarios	1	1	1	1	4 (100–220%)
DG types	PV only	Limited	Limited	PV + ESS	5 (Wind + PV + Synch)
Network reconfiguration	No	No	No	No	Yes (HSA)
Recon-fig.–protection coupling	No	No	No	No	Yes
Statistical validation	Yes	Yes (20 runs)	Yes (20 runs)	No	Deterministic (exact LP)
IEC Std. Inverse	Yes	Yes	Yes	Yes	Yes

Table 12. Statistics of the hybrid GA–SQP over ten independent runs.

Load (%)	CTI (s)	GA Only, Mean	GA–SQP, Mean	GA–SQP, std	GA–SQP, Best	Feasible Runs
100	0.2	19.88	18.40	0.00	18.40	10/10
100	0.3	29.16	26.43	0.00	26.43	10/10
140	0.2	21.60	19.47	0.00	19.47	10/10
140	0.3	30.16	28.08	0.00	28.08	10/10
180	0.2	21.26	19.04	0.00	19.04	10/10
180	0.3	29.56	27.38	0.00	27.38	10/10
220	0.2	20.19	18.14	0.00	18.14	10/10
220	0.3	28.05	26.01	0.00	26.01	10/10

6. Conclusions

The present study proposed a two-stage optimization framework for the synchronized reconfiguration of networks and the coordination of directional overcurrent relays in ADNs with substantial DG integration. The suggested framework combines the traditionally separate problems of operational efficiency and protection performance into one optimization model. This helps ensure that steady-state power-flow behavior and fault-response characteristics remain consistent across different operational scenarios.

Initially, the HSA was employed to achieve the ideal reconfiguration of an IEEE 33-bus test system incorporating five distributed generation units (two DFIG wind units, two photovoltaic units, and one synchronous generator) across four loading conditions. The reconfiguration diminished the active power loss by 21.42%, 28.24%, 31.70%, and 33.88% at loading levels of 100%, 140%, 180%, and 220%, respectively, while elevating

the minimum bus voltage above 0.90 pu in each scenario; the same configurations were obtained in repeated HSA runs with different random seeds, and optimality is not claimed for larger distribution networks. Although the absolute losses increase with loading (from 82.74 kW to 668.80 kW before reconfiguration), the percentage loss reduction achieved by reconfiguration also increases, indicating that the benefits of reconfiguration grow with demand. The load-dependent nature of the ideal configuration underscores the importance of dynamic topology optimization in heavily loaded distribution networks. Research indicates that a network design optimized without distributed generation (DG) results in a 25.6–33.9% increase in losses when DG units are integrated, underscoring the necessity of including DG in the reconfiguration challenge.

In the subsequent phase, relay coordination for the restructured network was developed based on a positive-sequence short-circuit analysis that incorporated input from each type of distributed generation. Due to the constancy of the pickup currents and the IEC standard inverse characteristic, the coordination of the TDS values constitutes a linear programming problem; it was resolved using the hybrid GA–SQP algorithm, which yielded results that aligned with the precise linear-programming optimum in every instance. Zero CTI violations were recorded for the 32 relays supplied by substations and the 31 primary–backup pairs across all four loading levels, maintaining a CTI of 0.2 s. The cumulative primary operating durations were 18.40, 19.47, 19.04, and 18.14 s with loadings of 100%, 140%, 180%, and 220% (0.57–0.61 s per relay), and ranged from 26.0 to 28.1 s with a CTI of 0.3 s applied. The TDS measurements remain below 0.65, therefore comfortably within the acceptable limits, and the maximum primary operational duration of any relay is 1.36 s.

The issues of reconfiguration and coordination are interrelated: under nominal load, the nearly optimal configuration {7, 11, 12, 26, 36} incurs a loss that is merely 2.2% greater than the optimal (66.48 kW compared to 65.02 kW) while simultaneously decreasing the total primary operating duration from 18.40 s to 16.76 s (CTI = 0.2 s), representing an 8.9% reduction. This shows that the sequential approach, which fixes the loss-optimal topology first, is not jointly optimal; a joint search over near-optimal topologies could trade a small increase in losses for faster protection and is left for future work. The research is confined to balanced three-phase faults occurring at the midpoint of the lines, adhering to a predetermined pickup criterion, and presuming that the DG units are isolated by their own islanding protection post-fault; incorporating relays solely powered by the DG units into the coordination results in an increase in the total primary operating duration from 18.40 s to 34.91 s due to the minimal fault currents from the DG and the extensive relay chains they generate. The findings are obtained for four deterministic loading levels: the stochastic variation in wind generation, PV output, and load is not included and is left for future work. Likewise, faults at other locations, other fault types, fault resistance, and other DG operating states were not evaluated and would alter the fault-current ratios.

Multiple avenues for future research are described. Adding unbalanced three-phase modeling would help to better represent real-world DN with asymmetric loading and single-phase laterals. Moreover, adding battery energy storage systems and DR resources to the co-optimization framework for reconfiguration and protection would make the grid more resilient and flexible when there is significant renewable energy. Finally, adaptive or learning-based protection schemes that adjust relay settings online using real-time measurements and machine learning appear to be a promising approach to improving protection when DG output changes rapidly. This is especially true when communication delays and cybersecurity issues are factored in. In the end, using real utility data for hardware-in-the-loop experimental validation would make it easier to move from simulation results to real-world use, thereby demonstrating that the proposed framework is useful for real-world ADNs applications.

Author Contributions: Conceptualization, H.S. and E.K.Y.; methodology, H.S.; software, H.S.; validation, E.K.Y.; formal analysis, H.S.; investigation, H.S.; resources, E.K.Y.; data curation, H.S.; writing—original draft preparation, H.S.; writing—review and editing, E.K.Y.; visualization, H.S.; supervision, E.K.Y.; project administration, E.K.Y. All authors have read and agreed to the published version of the manuscript.

Funding: This research received no external funding.

Data Availability Statement: The data and custom codes used to support the findings of this study are available from the corresponding author upon reasonable request. The code is currently part of an ongoing Ph.D. research project and will be made publicly available upon the completion of the study.

Conflicts of Interest: The authors declare no conflicts of interest regarding the publication of this paper. No funding was received for conducting this study, and the authors have no relevant financial or non-financial interests to disclose.

Abbreviations

DG	Distributed Generation
RES	Renewable energy resources
DNR	Distribution network reconfiguration
HSA	Harmony Search Algorithm
CTI	Coordination Time Interval
GA	Genetic Algorithm–
SQP	Sequential Quadratic Programming
HHO	Harris Hawks Optimization
TDS	Time Dial Settings
DN	Distribution networks
ADNs	Modern active distribution networks
PV	Photovoltaic
MINLP	Mixed-Integer Nonlinear Programming
MILP	Mixed-Integer Linear Programming
SOCP	Second-Order Cone Programming
PSO	Particle Swarm Optimization
ACO	Ant Colony Optimization
CS	Cuckoo Search
FA	Firefly Algorithm
HMS	Harmony Memory Stores
PAR	Pitch Adjustment Rate
DFIGs	Doubly Fed Induction Generators
IIDGs	Inverter-Interfaced Distributed Generators
PCP	Protection Coordination Problem
SSA	Salp Swarm Algorithm
OP	Quadratic Programming
BFGS	Broyden-Fletcher-Goldfarb-Shanno
KKT	Karush-Kuhn-Tucker
SBX	Simulated Binary Crossover

References

1. Azizi, A.; Vahidi, B.; Nematollahi, A.F. Reconfiguration of active distribution networks equipped with soft open points considering protection constraints. *J. Mod. Power Syst. Clean Energy* **2023**, *11*, 212–222. [CrossRef]
2. Khorram-Nia, R.; Bahmani-Firouzi, B.; Simab, M. Optimal scheduling of reconfigurable microgrids incorporating the PEVs and uncertainty effects. *IET Renew. Power Gener.* **2022**, *16*, 3531–3543. [CrossRef]
3. Wong, J.; Tan, C.; Abd Rahim, N.; Tan, R.H. Communication-less adaptive overcurrent protection for highly reconfigurable systems based on nonparametric load flow models. *IEEE Trans. Power Deliv.* **2023**, *39*, 202–209. [CrossRef]
4. Esmaeili, S.; Anvari-Moghaddam, A.; Jadid, S.; Guerrero, J.M. Optimal simultaneous day-ahead scheduling and hourly reconfiguration of distribution systems considering responsive loads. *Int. J. Electr. Power Energy Syst.* **2019**, *104*, 537–548. [CrossRef]
5. Mohamedshareef, R.; Abapour, M.; Hosseini, S.H.; Seyedi, H. Optimal overcurrent relay coordination: Balancing costs, time performance and generator placement in fault current limiter optimization. *IET Gener. Transm. Distrib.* **2024**, *18*, 1431–1448. [CrossRef]

6. Yousaf, M.; Jalilian, A.; Muttaqi, K.M.; Sutanto, D. An adaptive overcurrent protection scheme for dual-setting directional recloser and fuse coordination in unbalanced distribution networks with distributed generation. *IEEE Trans. Ind. Appl.* **2022**, *58*, 1831–1842. [CrossRef]
7. Shobole, A.A.; Abafogi, M.; Zaim, A.; Amireh, Y. Multi agent system based adaptive numerical relay design and development, Part II: Hardware. *Electr. Power Syst. Res.* **2024**, *226*, 109889. [CrossRef]
8. Acevedo-Iles, M.; Romero-Quete, D.; Cortes, C.A. A Distributed Coordination Approach for Enhancing Protection System Adaptability in Active Distribution Networks. *Energies* **2024**, *17*, 4338. [CrossRef]
9. Al-Bhadely, F.; İnan, A. Improving directional overcurrent relay coordination in distribution networks for optimal operation using hybrid genetic algorithm with sequential quadratic programming. *Energies* **2023**, *16*, 7031. [CrossRef]
10. Ntshiba, S.; Krishnamurthy, S.; Nomandela, S. HIL simulation and testing of the distribution network's automatic reconfiguration. In *IEEE PES/IAS PowerAfrica*; IEEE: New York, NY, USA, 2024.
11. Akin, F.; Dinc, M.; Arikan, O. *DG* Optimization in Power Systems Considering Power Losses and CB Rating Violations. In *2025 7th Global Power, Energy and Communication Conference (GPECOM)*; IEEE: New York, NY, USA, 2025.
12. Khoshbakht, E.; Namdari, F.; Doostizadeh, M. Effects of protection settings on optimal performance of reconfigurable smart distribution systems. *IET Renew. Power Gener.* **2021**, *15*, 1678–1692. [CrossRef]
13. Rahim, M.N.A.; Mokhlis, H.; Bakar, A.H.A.; Rahman, M.T.; Badran, O.; Mansor, N.N. Protection coordination toward optimal network reconfiguration and DG sizing. *IEEE Access* **2019**, *7*, 163700–163718. [CrossRef]
14. Rezaei, M.F.; Ghobadpour, S. Reconfiguration of the real distribution network and providing a new resilience index, considering the uncertainty of renewable energy sources and digital protection devices in order to improve the resilience. *Electr. Power Syst. Res.* **2024**, *228*, 110012. [CrossRef]
15. Mohammedi, R.D.; Gozim, D.; Kouzou, A.; Mosbah, M.; Hafaifa, A.; Rodriguez, J.; Abdelrahem, M. Simultaneous Optimization of Network Reconfiguration and Soft Open Points Placement in Radial Distribution Systems Using a Lévy Flight-Based Improved Equilibrium Optimizer. *Energies* **2024**, *17*, 5911. [CrossRef]
16. He, M.; Wang, Y.; Song, Z.; Tan, Z.; Cai, Y.; You, X.; Xie, G.; Huang, X. Power Quality Mitigation in Modern Distribution Grids: A Comprehensive Review of Emerging Technologies and Future Pathways. *Processes* **2025**, *13*, 2615. [CrossRef]
17. Júnior, V.F.; Ferraz, R.S.; Ferraz, R.S.; Rueda-Medina, A.C.; Palmeira, E.S. Allocation and Sizing of Distributed Energy Resources and Capacitor Banks Considering Network Reconfiguration through Multi-objective Optimization Algorithms. *IEEE Access* **2026**, *14*, 70941–70954. [CrossRef]
18. Lotfi, H.; Shojaei, A.A. A dynamic model for multi-objective feeder reconfiguration in distribution network considering demand response program. *Energy Syst.* **2023**, *14*, 1051–1080. [CrossRef]
19. Kahnamouei, A.S.; Lotfifard, S.; Rostami, M. Optimized distribution systems reconfiguration considering protection devices constraints. *IEEE Trans. Power Deliv.* **2025**, *40*, 1267–1278. [CrossRef]
20. Xie, B.; Zhao, D.; Hong, T. Transformer monitoring and protection in dynamic power systems—A review. *Front. Energy Res.* **2020**, *8*, 150. [CrossRef]
21. Apostolopoulos, C.A.; Arsoniadis, C.G.; Georgilakis, P.S.; Nikolaidis, V.C. Unsynchronized measurements based fault location algorithm for active distribution systems without requiring source impedances. *IEEE Trans. Power Deliv.* **2021**, *37*, 2071–2082. [CrossRef]
22. Arévalo, P.; Jurado, F. Impact of artificial intelligence on the planning and operation of distributed energy systems in smart grids. *Energies* **2024**, *17*, 4501. [CrossRef]
23. Kamarposhti, M.A.; Shokouhandeh, H.; Lee, Y.; Kang, S.K.; Colak, I.; Barhoumi, E.M. Optimizing energy management in microgrids with ant colony optimization: Enhancing reliability and cost efficiency for sustainable energy systems. *Int. J. Low.-Carbon Technol.* **2024**, *19*, 2848–2856. [CrossRef]
24. Suraya, S.; Irshad, S.M.; Ramesh, G.P.; Sujatha, P. Biogeography based optimization algorithm and neural network to optimize place and size of distributed generating system in electrical distribution. *J. Electr. Eng. Technol.* **2022**, *17*, 1593–1603. [CrossRef]
25. Ghanbari, M.; Gandomkar, M.; Nikoukar, J. Protection coordination of bidirectional overcurrent relays using developed particle swarm optimization approach considering distribution generation penetration and fault current limiter placement. *IEEE Can. J. Electr. Comput. Eng.* **2021**, *44*, 143–155. [CrossRef]
26. Foqha, T.; Alsadi, S.; Omari, O.; Refaat, S.S. Optimization techniques for directional overcurrent relay coordination: A comprehensive review. *IEEE Access* **2023**, *12*, 1952–2006. [CrossRef]
27. Ghiasi, M.; Wang, Z.; Mehrandezh, M.; Alhelou, H.H.; Ghadimi, N. Enhancing power grid stability: Design and integration of a fast bus tripping system in protection relays. *IEEE Trans. Consum. Electron.* **2024**, *71*, 561–570. [CrossRef]
28. Alasali, F.; El-Naily, N.; Mustafa, H.Y.; Loukil, H.; Saad, S.M.; Saidi, A.S.; Holderbaum, W. Advanced voltage relay design for distance relay coordination in power networks equipped with low-inertia areas. *IET Gener. Transm. Distrib.* **2025**, *19*, e13338. [CrossRef]

29. Otuo-Acheampong, D.; Rashed, G.I.; Akwasi, A.M.; Haider, H. Application of Optimal Network Reconfiguration for Loss Minimization and Voltage Profile Enhancement of Distribution System Using Heap-Based Optimizer. *Int. Trans. Electr. Energy Syst.* **2023**, *2023*, 9930954. [CrossRef]
30. Su, Y.; Hu, Q.; Tian, Y.; Dai, R.; Lv, Z.; Zhang, M. Distribution network reconfiguration based on hybrid particle swarm optimization and Grey wolf optimization. In *2023 IEEE 7th Conference on Energy Internet and Energy System Integration (EI2)*; IEEE: New York, NY, USA, 2023.
31. Reiz, C.; Alves, E.; Melim, A.; Gouveia, C.; Carrapatoso, A. Novel adaptive protection approach for optimal coordination of directional overcurrent relays. In *2024 IEEE 22nd Mediterranean Electrotechnical Conference (MELECON)*; IEEE: New York, NY, USA, 2024.
32. Rajput, V.N.; Pandya, K.S. A hybrid improved harmony search algorithm-nonlinear programming approach for optimal coordination of directional overcurrent relays including characteristic selection. *Int. J. Power Energy Convers.* **2018**, *9*, 228–253. [CrossRef]
33. Mishra, A.; Tripathy, M.; Ray, P. A survey on different techniques for distribution network reconfiguration. *J. Eng. Res.* **2024**, *12*, 173–181. [CrossRef]
34. Neda, O.M. Hybrid design of optimal reconfiguration and DG sizing and siting using a novel improved salp swarm algorithm. *Electr. Eng.* **2025**, *107*, 14159–14174. [CrossRef]
35. Vasconcelos, L.H.P.; Almeida, A.R.; dos Santos, B.F., Jr.; Melo, N.X.; Carvalho, J.G.S.; de Oliveira Sobreira, D. Hybrid optimization algorithm applied to adaptive protection in distribution systems with distributed generation. *Electr. Power Syst. Res.* **2022**, *202*, 107605. [CrossRef]
36. Al-Bhadely, F.; İnan, A. Enhancing coordination efficiency with fuzzy monte carlo uncertainty analysis for dual-setting directional overcurrent relays amid distributed generation. *Sensors* **2024**, *24*, 4109. [CrossRef] [PubMed]
37. Linh, N.T. A novel combination of genetic algorithm, particle swarm optimization, and teaching-learning-based optimization for distribution network reconfiguration in case of faults. *Eng. Technol. Appl. Sci. Res.* **2024**, *14*, 12959–12965. [CrossRef]
38. Parihar, S.S.; Malik, N. Network reconfiguration in the presence of optimally integrated multiple distributed generation units in a radial distribution network. *Eng. Optim.* **2024**, *56*, 679–699. [CrossRef]
39. Swaminathan, D.; Rajagopalan, A.; Montoya, O.D.; Arul, S.; Grisales-Noreña, L.F. Distribution network reconfiguration based on hybrid golden flower algorithm for smart cities evolution. *Energies* **2023**, *16*, 2454. [CrossRef]
40. Jayabarathi, T.; Raghunathan, T.; Mithulananthan, N.; Cherukuri, S.H.C.; Sai, G.L. Enhancement of distribution system performance with reconfiguration, distributed generation and capacitor bank deployment. *Heliyon* **2024**, *10*, e26343. [CrossRef] [PubMed]
41. Moghari, P.; Chabanloo, R.M.; Torkaman, H. Distribution system reconfiguration based on MILP considering voltage stability. *Electr. Power Syst. Res.* **2023**, *222*, 109523. [CrossRef]
42. Sati, T.E.; Azzouz, M.A. An adaptive virtual impedance fault current limiter for optimal protection coordination of islanded microgrids. *IET Renew. Power Gener.* **2022**, *16*, 1719–1732. [CrossRef]
43. ElSayed, S.K.; Elattar, E.E. Hybrid Harris hawks optimization with sequential quadratic programming for optimal coordination of directional overcurrent relays incorporating distributed generation. *Alex. Eng. J.* **2021**, *60*, 2421–2433. [CrossRef]
44. Shrivastava, A.; Sharma, A.; Pandit, M.; Jately, V.; Azzopardi, B. Hybrid protection scheme based optimal overcurrent relay coordination strategy for RE integrated power distribution grid. *Energies* **2021**, *14*, 7192. [CrossRef]

Disclaimer/Publisher's Note: The statements, opinions and data contained in all publications are solely those of the individual author(s) and contributor(s) and not of MDPI and/or the editor(s). MDPI and/or the editor(s) disclaim responsibility for any injury to people or property resulting from any ideas, methods, instructions or products referred to in the content.